VILNIUS UNIVERSITY
AND
CENTER FOR PHYSICAL SCIENCES AND TECHNOLOGY

JULIJANAS ŽELUDEVIČIUS

OPTIMIZATION OF PULSED FIBER LASERS, NONLINEAR PULSE COMBINING AND OPTICAL FREQUENCY CONVERSION

Summary of doctoral thesis
Technological Sciences, Material Engineering (08T)

Vilnius, 2017

Doctoral thesis was prepared in 2012-2016 at the Department of Laser Technologies of the Center for Physical Sciences and Technology (FTMC).

Scientific supervisor:
Dr. Kęstutis Regelskis (Center for Physical Sciences and Technology, Technological Sciences, Material Engineering – 08T)

Doctoral thesis will be defended during open session of Doctoral Council:

Chairman:
Prof. Habil. Dr. Valerijus Smilgevičius (Vilnius University, Technological Sciences, Material Engineering – 08T).

Members:
Dr. Giedrius Andriukaitis (Photonics institute, TU Wien (Austria), Technological Sciences, Material Engineering – 08T);
Prof. Habil. Dr. Arūnas Krotkus (Center for Physical Sciences and Technology, Technological Sciences, Material Engineering – 08T);
Dr. Andrejus Michailovas (Center for Physical Sciences and Technology, Technological Sciences, Material Engineering – 08T);
Dr. Sergejus Orlovas (Center for Physical Sciences and Technology, Technological Sciences, Material Engineering – 08T).

This thesis will be under open consideration on 29th of September 2017 at 10 a.m. in the Hall of FTMC Institute of Physics.

Address: Savanoriu Ave. 231, LT-02300 Vilnius, Lithuania.

Summary of doctoral thesis was distributed on 29th of August 2017.

Doctoral thesis is available at the libraries of Vilnius University and Center for Physical Sciences and Technology, and accessible by link www.vu.lt/lt/naujienos/ivykiu-kalendorius.

VILNIAUS UNIVERSITETAS
IR
VALSTYBINIS MOKSLINIŲ TYRIMŲ INSTITUTAS
FIZINIŲ IR TECHNOLOGIJOS MOKSLŲ CENTRAS

JULIJANAS ŽELUDEVIČIUS

IMPULSINIŲ SKAIDULINIŲ LAZERIŲ PARAMETRŲ OPTIMIZAVIMAS, NETIESINIS IMPULSŲ APJUNGIMAS IR OPTINIO DAŽNIO KEITIMAS

Daktaro disertacijos santrauka
Technologijos mokslai, Medžiagų inžinerija (08T)

Vilnius, 2017

Disertacija rengta 2012–2016 metais Valstybinio mokslinių tyrimų instituto Fizinių ir technologijos mokslų centro Lazerinių technologijų skyriuje.

Mokslinis vadovas – dr. Kęstutis Regelskis (Fizinių ir technologijos mokslų centras, technologijos mokslai, medžiagų inžinerija – 08T).

Disertacija ginama viešame Gynimo tarybos posėdyje:

Pirmininkas – prof. habil. dr. Valerijus Smilgevičius (Vilniaus universitetas, technologijos mokslai, medžiagų inžinerija – 08T).

Nariai:
Dr. Giedrius Andriukaitis (Fotonikos institutas, Vienos technologijų universitetas, Austrija, technologijos mokslai, medžiagų inžinerija – 08T);
Prof. habil. dr. Arūnas Krotkus (Fizinių ir technologijos mokslų centras, technologijos mokslai, medžiagų inžinerija – 08T);
Dr. Andrejus Michailovas (Fizinių ir technologijos mokslų centras, technologijos mokslai, medžiagų inžinerija – 08T);
Dr. Sergejus Orlovas (Fizinių ir technologijos mokslų centras, technologijos mokslai, medžiagų inžinerija – 08T).

Disertacija bus ginama viešame disertacijos Gynimo tarybos posėdyje 2017 m. rugsėjo mėn. 29 d. 10 val. FTMC Fizikos instituto salėje.

Adresas: Savanorių pr. 231, LT-02300 Vilnius, Lietuva.

Disertacijos santrauka išsiuntinėta 2017 m. rugpjūčio 29 d.

Disertaciją galima peržiūrėti Vilniaus universiteto, Fizinių ir technologijos mokslų centro bibliotekose ir VU interneto svetainėje adresu: www.vu.lt/lt/naujienos/ivykiu-kalendorius.

TABLE OF CONTENTS

Acknowledgements

First, I am very grateful to my advisor Dr. Kęstutis Regelskis for transferring his knowledge and experience, for new scientific ideas and for all his support in the research. Also, I am grateful for providing opportunities to work using newest laboratory equipment, take part in internships and international conferences.

Furthermore, I am grateful to chief of our department Dr. Gediminas Račiukaitis for consulting on scientific and organizational matters. Also, for constant work allowing to achieve good results in our department.

I would also like to thank to other colleagues of our department for friendly work atmosphere.

Moreover, I would like to thank the fiber technology group of company Ekspla, headed by Dr. Nerijus Rusteika, for cooperation. Especially to Dr. Rokas Danilevičius for help in the modelling of fiber laser systems, discussions on scientific and non-scientific matters. Also, I am grateful to Dr. Karolis Viskontas and PhD student Saulius Frankinas for opportunities to borrow required equipment.

Finally, I am very grateful to my parents for their constant support.

List of abbreviations

AOM	acousto-optic modulator
ASE	amplified spontaneous emission
BBO	Beta-Barium Borate (β-BaB$_2$O$_4$)
CCC	chirally coupled core
CPA	chirped pulse amplification
DC	double clad
FBG	fiber Bragg grating
FCPA	fiber chirped pulse amplification
FWHM	full width at half maximum
FWM	four-wave mixing
GVD	group velocity dispersion
KTP	Potassium Titanyl Phosphate (KTiOPO$_4$)
LBO	Lithium Triborate (LiB$_3$O$_5$)
LD	laser diode
LMA	large mode area
NA	numerical aperture
PER	polarization extinction ratio
PM	polarization maintaining
SHG	second harmonic generation
SM	single-mode
SRS	stimulated Raman scattering
TOD	third-order dispersion
WDM	wavelength division multiplexer
Yb	Ytterbium

Introduction

First applications of optical fibers were in the telecommunications field, as a replacement for copper transmission lines. Especially after refinement of manufacturing technologies of low-loss rare-earth-doped fibers [1] and development of pump diodes suitable for pumping of such active medium. Initial interest in fibers as a medium for laser operation was caused by inherent to such lasers properties of compactness and stability. After a demonstration of double-clad fiber [2], the rapid development of high-average-power fiber lasers has begun. Advantages of fiber geometry such as outstanding thermo-optical properties and perfect beam quality, because of confined propagation, allowed for an exponential increase of average power output from the fiber lasers. Particularly good results were achieved using ytterbium-doped fibers because of the achievable low quantum defect between the pump and emitted radiation [3]. Additional power increase was achieved by implementing tandem pumping methods [4]. Because of persistent developments, currently, more than 10 kW average power is achieved from the single-mode fiber laser [5].

Although generation of ultrashort pulses in the fiber lasers was demonstrated shortly after CW operation demonstration of the fiber laser [6,7], scaling of pulse peak power was not so straightforward. Same properties of fiber geometry, which allow for good heat removal and immunity to high average power operation, are unfavorable for high-peak-power pulses. Because of confinement of radiation in a small diameter core and long interaction lengths, maximum peak power achievable in fiber is limited by nonlinear effects. In order to avoid these limitations, different methods allowing for the reduction of peak irradiances in the fiber were proposed and implemented. A lot of work was done designing novel fibers suitable for high-peak-power operation [8,9], improving chirped pulse amplification methods [10,11], and creating methods for combining of radiation from the multiple fiber lasers [12,13]. At the same time, it was aimed to preserve inherent for the fiber lasers features of high efficiency, compactness, stability, tuning-free operation. Such reliable ultrashort pulse sources are needed for fast and precision material micromachining [14–16], modifications of transparent materials and manufacture of photonic structures [17], pumping of parametrical generators [18] and generation of terahertz radiation [19,20]. Recently, the ambitious long-term goal was introduced, which envisages usage of fiber laser architecture and implementation of beam combining techniques to achieve an extreme peak and average power pulses (100 TW, 100 kW) for particle acceleration research [21]. Achieving such goals requires investigation aimed to improve average and peak power pulse characteristics from the fiber lasers.

The research described in this thesis was aimed at optimization of pulse characteristics achievable from fiber lasers. Two approaches were investigated: optimization of pulse parameters emitted directly from fibers (for highest pulse energy and shortest pulse duration) and external pulse modification by frequency conversion in quadratic susceptibility nonlinear crystal. Demand for shorter wavelength pulses than are generated in Yb-doped medium arise from applications in material processing field [22]. According to the first approach, novel pulse generation method in fiber was investigated, which relies on self-phase modulation in fiber and double-alternating spectral filtering, and allows generating ultrashort high-energy pulses (chapter 2). Additionally, pulse amplification in fiber amplifier to highest achievable pulse energy was investigated using chirped pulse

amplification methods (chapter 3). According to second approach, method for efficient second harmonic generation of broadband pulsed radiation in nonlinear crystal with longitudinal temperature gradient was investigated (chapter 4). Finally, two methods allowing for combining of pulsed radiation from fiber lasers and together performing optical frequency conversion were investigated (chapter 5).

Aim and the main tasks of the thesis

The aim of this work was to investigate and optimize methods allowing for generation and amplification of pulses in fiber lasers and to achieve best possible pulse characteristics (shortest pulse duration, highest pulse energy). Also, to optimize frequency conversion of broadband pulsed radiation from fiber lasers in quadratic susceptibility crystals by investigating novel second harmonic generation method based on imposing temperature gradient along nonlinear crystal. Finally, to investigate combining of radiation from multiple fiber lasers together with accomplishing frequency conversion in order to achieve pulsed radiation with better characteristics (average and peak power) than from the single fiber laser. Main tasks:

1. To investigate a method for pulse generation in fiber lasers, based on spectral broadening, caused by self-phase modulation of pulses in fiber, and double-alternating spectral filtering.
2. To investigate capabilities and properties of chirped pulse amplification method using fiber amplifiers with different core diameter and operating at high levels of self-phase modulation.
3. To investigate a method for efficient second harmonic generation of broadband (chirped) pulses, generated in fiber lasers, by imposing temperature gradient along quadratic susceptibility crystal.
4. To investigate a method for combining of pulsed radiation from fiber lasers by utilizing properties of non-collinearly phase-matched sum-frequency generation.
5. To investigate a method for combining two, separated in time, pulses of the same beam by frequency conversion in quadratic susceptibility crystal.

Novelty and importance of the work

- Novel and perspective method for generation of ultrashort pulses in optical fiber lasers was investigated. The method is based on cubic nonlinearity of the fiber and thus does not require other materials with saturable losses, which usually induce additional limitations to the operation of such lasers. By using mentioned method, reliable, long-lifetime pulsed light sources can be designed, and this is very important for practical applications.
- A method of chirped pulse amplification in fibers was demonstrated, in which self-phase modulation effect was utilized both in pulse stretcher and pulse amplification stages. Simple chirped pulse amplification system was demonstrated, which, after optimization, can provide high energy femtosecond pulses.
- A novel method for second harmonic generation of broadband pulsed radiation from fiber lasers, by setting temperature gradient along quadratic susceptibility crystal, was demonstrated. Such method can be applied to design universal optical frequency

conversion modules suitable for input wavelengths corresponding to whole Yb-doped fused silica emission band.

- Two novel methods for pulse combining and optical frequency conversion of pulses from fiber lasers in quadratic susceptibility crystal were investigated. One method allows combining pulses from multiple fiber lasers into one sum-frequency beam and in such way increase pulse repetition rate and average power. Another method allows to combine two pulses, separated in time, into the single pulse and in such way increase pulse energy and peak power. These methods can be potentially used for generation of laser radiation with average/peak power higher than achievable in the single fiber amplifier.

Statements to defend

1. Stable ultrashort pulses with relatively high energy and wavelength in the range of Yb-doped fused silica can be generated by utilizing spectral broadening of pulses caused by self-phase modulation in fiber and double-alternating spectral filtering.
2. Nonlinear FCPA system in which self-phase modulation is utilized both in pulse stretcher and pulse amplification stages, after optimization, allows to generate pulses with a shorter duration than the duration of initial oscillator-seeder pulses, and with higher energy than achievable in linear operation regime for corresponding mode field area fiber amplifier.
3. By using LBO crystal in the setup with a longitudinal temperature gradient, significantly higher conversion to the second harmonic efficiency of broadband pulses from fiber lasers can be achieved than using conventional SHG configuration in which crystal temperature is uniform. When using this method, it is not necessary to optimize crystal length because conversion process is unidirectional and back-conversion does not occur even when crystal length is much bigger than optimal.
4. Pulsed optical beams from multiple fiber amplifiers can be combined in pairs into a single beam in which pulses are multiplexed in time by using noncollinear sum-frequency generation technique. The average power of combined beam is proportional to a number of combined fiber amplifiers, and spatial characteristics of the combined beam are not worse than characteristics of beams generated in corresponding fiber amplifiers.
5. The sequential combining of a pair of pulses in quadratic susceptibility crystal allows generating sum-frequency pulses with higher energy and peak power than in the case when optical frequency conversion is accomplished using conventional SHG configuration.

Author's contribution

Experiments described in this thesis were conducted in Laser Technology Department of Center for Physical Sciences and Technology during the period of 2012-2016. Author has constructed almost all described experimental setups, conducted measurements, analyzed experimental data with respect to numerical models and prepared publications. Co-authors' contribution is indicated in the following subsection.

Co-authors' contribution

- Dr. Kęstutis Regelskis headed entire research work process, introduced new research directions, advised on scientific matters and strongly contributed to the preparation of scientific publications S1, S3 and P1.
- Dr. Gediminas Račiukaitis consulted on the preparation of publications.
- Dr. Rokas Danilevičius carried out modelling of chirped pulse amplification system described in S2.
- Dr. Karolis Viskontas constructed fiber oscillator used in chirped pulse amplification system investigations described in S2.
- Dr. Nerijus Rusteika contributed to the preparation of publication S2.
- Marijus Mickus carried out experimental measurements of pulse generator scheme with fiber Bragg gratings.
- Martynas Dapkus carried out an experimental investigation of the self-starting operation of pulse generator scheme.

Scientific papers

Scientific papers related to the topic of the thesis:

S1.	K. Regelskis, **J. Želudevičius**, N. Gavrilinas, and G. Račiukaitis, "Efficient second-harmonic generation of a broadband radiation by control of the temperature distribution along a nonlinear crystal," Optics Express **20**, 28544–28556 (2012).

S2.	**J. Želudevičius**, R. Danilevičius, K. Viskontas, N. Rusteika, and K. Regelskis, "Femtosecond fiber CPA system based on picosecond master oscillator and power amplifier with CCC fiber," Optics Express **21**, 5338–5345 (2013).

S3.	K. Regelskis, **J. Želudevičius**, K. Viskontas, and G. Račiukaitis, "Ytterbium-doped fiber ultrashort pulse generator based on self-phase modulation and alternating spectral filtering," Optics Letters **40**, 5255–5258 (2015).

S4.	**J. Želudevičius**, K. Regelskis, and G. Račiukaitis, "Experimental demonstration of pulse multiplexing and beam combining of four fiber lasers by noncollinear frequency conversion in an LBO crystal," Optics Letters **42**, 175–178 (2017).

Other scientific papers:

S5.	**J. Želudevičius**, R. Danilevičius, and K. Regelskis, "Optimization of pulse compression in a fiber chirped pulse amplification system by adjusting dispersion parameters of a temperature-tuned chirped fiber Bragg grating stretcher," Journal of the Optical Society of America B **32**, 812–817 (2015).

Patent application related to the topic of the thesis:

P1.	K. Regelskis, **J. Želudevičius**, and G. Račiukaitis, "Šviesos impulsų suminio dažnio generavimo būdas." Patent of Lithuania Nr. LT 5968. "Method and device for sum-frequency generation of light pulses," European patent application EP2621032 (A2).

Conference presentations

Presentations directly related to the topic of the thesis:
Name of the presenting author is underlined.

K1.	**<u>J. Želudevičius</u>**, K. Regelskis, V. Vosylius, N. Gavrilinas, and G. Račiukaitis, "Enhancement of the second-harmonic phase-matching bandwidth and conversion

efficiency by control of the temperature distribution along a nonlinear crystal," *Advanced Solid-State Photonics (ASSP)*, San Diego, USA (2012).

K2. K. Regelskis, **J. Želudevičius**, N. Gavrilinas, and G. Račiukaitis, "Combining of pulses in time domain by second harmonic generation," *Advanced Solid-State Photonics (ASSP)*, San Diego, USA (2012).

K3. **J. Želudevičius**, R. Danilevičius, K. Viskontas, N. Rusteika and K. Regelskis, "Femtosecond fiber CPA system seeded by bandwidth-limited picosecond pulses," *2013 Conference on Lasers and Electro-Optics Europe and International Quantum Electronics Conference (CLEO EUROPE/IQEC)*, Munich, Germany (2013). DOI: 10.1109/CLEOE-IQEC.2013.6801097

K4. **J. Želudevičius**, K. Regelskis, N. Gavrilin, and G. Račiukaitis, "Efficient second-harmonic generation of broadband radiation in the nonlinear crystal with constant axial temperature gradient," *2013 Conference on Lasers and Electro-Optics Europe and International Quantum Electronics Conference (CLEO EUROPE/IQEC)*, Munich, Germany (2013). DOI:10.1109/CLEOEIQEC.2013.6800929

K5. **J. Želudevičius**, K. Regelskis, N. Gavrilin, G. Raciukaitis, "Efficient second-harmonic generation of broadband light pulses in the LBO nonlinear crystal with constant axial temperature gradient," *XX Lietuvos-Baltarusijos seminaras "Lazeriai ir optinis nietiesiškumas"*, Vilnius, Lietuva (2013).

K6. R. Danilevičius, **J. Želudevičius**, K. Viskontas, N. Rusteika, K. Regelskis. "Femtosecond fiber CPA system seeded by bandwidth-limited picosecond pulses: numerical and experimental study," *XX Lietuvos-Baltarusijos seminaras "Lazeriai ir optinis nietiesiškumas"*, Vilnius, Lietuva (2013).

K7. **J. Želudevičius**, R. Danilevičius, K. Viskontas, N. Rusteika, and K. Regelskis, "Performance of nonlinear ultra-short pulse fiber CPA system using power amplifiers with core diameter from 12 to 33 µm," *2014 International Conference "Laser Optics"*, St. Petersburg, Russia (2014). DOI:10.1109/LO.2014.6886281

K8. K. Regelskis, **J. Želudevičius**, and V. Žvirblyte, "Peculiarities of second harmonics generation with linearly varying wave-number mismatch along a nonlinear crystal," *2014 International Conference "Laser Optics"*, St. Petersburg, Russia (2014). DOI:10.1109/LO.2014.6886405

K9. **J. Želudevičius**, R. Danilevičius, K. Viskontas, N. Rusteika, K. Regelskis, "Ultrashort-Pulse Nonlinear Fiber CPA System Performance Using Power Amplifiers with Core Diameter from 12.5 to 33 µm," *6th EPS-QEOD Europhoton Conference "Solid State, Fibre, and Waveguide Coherent Light Sources"*, Neuchatel, Switzerland (2014).

K10. **J. Želudevičius**, K. Regelskis, "Optimization of Nonlinear Fiber CPA System by Selection of Spectral Region of Operation," *6th EPS-QEOD Europhoton Conference "Solid State, Fibre, and Waveguide Coherent Light Sources"*, Neuchatel, Switzerland (2014).

K11. K. Regelskis, **J. Želudevičius**, G. Račiukaitis, "Picosecond fiber generator using a self-phase modulation and alternating spectral filtering," *6th EPS-QEOD Europhoton Conference "Solid State, Fibre, and Waveguide Coherent Light Sources"*, Neuchatel, Switzerland (2014).

K12. K. Regelskis, **J. Želudevičius**, V. Žvirblyte, G. Račiukaitis, "Peculiarities of second harmonics generation with a constant wave-number mismatch gradient along a

nonlinear crystal," *6th EPS-QEOD Europhoton Conference "Solid State, Fibre, and Waveguide Coherent Light Sources"*, Neuchatel, Switzerland (2014).

K13. K. Regelskis, **J. Želudevičius**, and G. Račiukaitis, "Stable operation of the picosecond pulse fiber generator based on a nonlinear spectral reshaping," *Northen Optics & Photonics 2015*, Lappeenranta, Finland (2015).

K14. **J. Želudevičius**, J. Petkelis, K. Regelskis, and G. Račiukaitis, "All-fiber Picosecond Optical Pulse Generator Based on Self-phase Modulation Effect and Spectral Filtering using Narrowband FBG," *European Conference on Lasers and Electro-Optics - European Quantum Electronics Conference (CLEO/Europe-EQEC 2015)*, Munich, Germany (2015).

K15. K. Regelskis, **J. Želudevičius**, and G. Račiukaitis, "Ultrashort Optical Pulse Yb-doped Fiber Generator Based on Nonlinear Spectral Re-shaping," *European Conference on Lasers and Electro-Optics - European Quantum Electronics Conference (CLEO/Europe-EQEC 2015)*, Munich, Germany (2015).

K16. **J. Želudevičius**, J. Petkelis, K. Regelskis, "Skaidulinio pikosekundinių impulsų generatoriaus, paremto fazes moduliavimosi reiškinio ir dvigubo spektrinio filtravimo naudojant siaurajuostes skaidulines Brego gardeles, tyrimai," *41-oji Lietuvos nacionalinė fizikos konferencija*, Vilnius, Lietuva (2015).

K17. K. Regelskis, **J. Želudevičius**, N. Gavrilinas, G. Račiukaitis, "Antros harmonikos generacijos ypatumų tyrimai esant pastoviam bangos skaičių nederinimo gradientui išilgai LBO kristalo," *41-oji Lietuvos nacionalinė fizikos konferencija*, Vilnius, Lietuva (2015)

K18. **J. Zeludevicius**, K. Regelskis, and G. Raciukaitis, "Combining and Temporal Multiplexing of Four Pulsed Beams from Fiber Amplifiers by Means of Non-collinear Frequency Conversion in KTP Crystal," *Conference on Lasers and Electro-Optics (2016)*, San Jose, USA, (2016). DOI:10.1364/CLEO_AT.2016.JTu5A.57

K19. **J. Želudevičius**, M. Mickus, and K. Regelskis, "Combining and temporal multiplexing of four pulsed beams in LBO crystal by means of non-collinear frequency conversion," *7th EPS-QEOD Europhoton Conference "Solid State, Fibre, and Waveguide Coherent Light Sources"*, Vienna, Austria (2016).

K20. **J. Želudevičius**, M. Mickus, and K. Regelskis, "Characterization of optical pulses generated by fiber pulse generators based on self-phase modulation and alternating spectral filtering," *7th EPS-QEOD Europhoton Conference "Solid State, Fibre, and Waveguide Coherent Light Sources"*, Vienna, Austria (2016).

Other presentations at conferences:

K21. R. Danilevičius, **J. Želudevičius**, K. Viskontas, N. Rusteika, and K. Regelskis, "Reduction of third order dispersion mismatch between fiber stretcher and grating compressor by using split-second-grating compressor design," *2014 International Conference "Laser Optics"*, St. Petersburg, Russia (2014). DOI:10.1109/LO.2014.6886277

K22. **J. Želudevičius**, R. Danilevičius, K. Regelskis, "Tuning of chirped fiber bragg grating pulse stretcher dispersion parameters by controlling temperature distribution," *Northen Optics & Photonics 2015*, Lappeenranta, Finland (2015).

Thesis summary

The thesis consists of 5 chapters, conclusions and a list of references. Thesis presented in 214 pages, contains 129 figures and 13 tables.

Chapter 1: Literature review

This chapter consists of 4 subchapters. In subchapter 1.1, material properties of the fused silica fibers are reviewed. Main attention is dedicated to linear and nonlinear material properties and their influence for propagating light pulses, especially with high peak power. Absorption, chromatic dispersion, nonlinear effects like self-phase modulation, stimulated Brillouin and Raman scattering, four-wave mixing and self-focusing are reviewed. Finally, description of pulse propagation in the single-mode fiber by means of nonlinear Schrödinger equation is briefly discussed.

In subchapter 1.2, fused silica fiber types and technologies are reviewed. Important properties of multimode, single-mode and polarization maintaining fibers are reviewed. Properties of Yb-doped fused silica active medium are described, and aspects of fibers for amplification of high-peak-power optical pulses are indicated. Types of active fibers for pulse amplification are reviewed, such as large mode area double clad fibers, photonic crystal fibers and higher-order mode filtering fibers, including chirally-coupled-core fiber.

In subchapter 1.3, optical frequency conversion in quadratic susceptibility crystals is reviewed. Description of the nonlinear process by means of the coupled-wave equation is presented. Phase-matching conditions both for collinear and non-collinear propagation are indicated, and calculation methods are described. Moreover, different effects, which are present when accomplishing frequency conversion of light pulses and have an influence on conversion efficiency, are reviewed. This includes effects of group velocity mismatch (temporal walk-off), spatial walk-off and influence of imperfect phase-matching at high conversion limit.

In subchapter 1.4, main techniques for ultrashort pulse generation in fibers are reviewed. Pulse formation mechanism based on pulse spectral broadening, caused by self-phase modulation in fiber, and alternating spectral filtering is introduced. Also pulse amplification in fiber techniques, particularly, chirped pulse amplification, are reviewed and significant achievements in these fields are highlighted. Moreover, methods for combining radiation from multiple fiber lasers, including nonlinear interaction, are reviewed. Finally, methods for improvement of frequency conversion of broadband radiation (in quadratic susceptibility medium) are reviewed.

Chapter 2: Research on fiber circuit for generation of high-energy pulses

In this chapter method for generation of ultrashort high-energy pulses in fiber is presented and investigated. Described method is based on pulse spectral broadening, caused by self-phase modulation (SPM) in fiber, and alternating spectral filtering.

First, a numerical model for the description of the linear pulse generating circuit is introduced. Schematic diagram of the circuit design described by this model is depicted in Fig. 1.
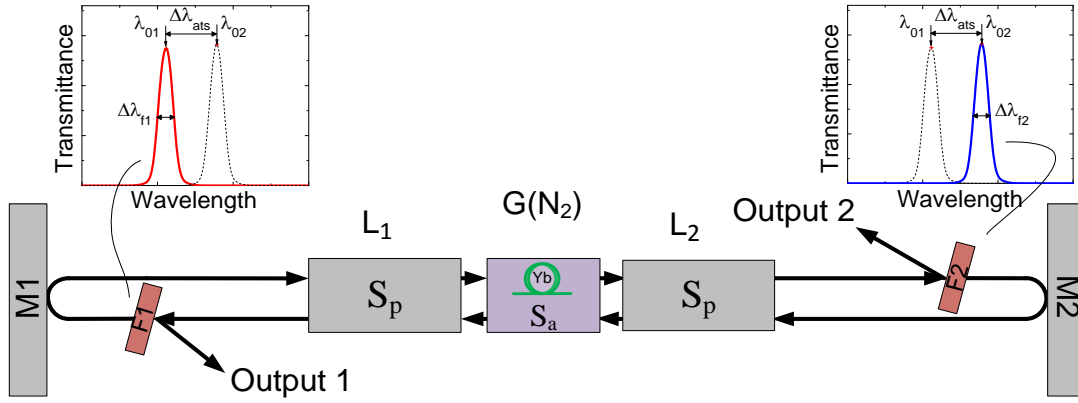
Fig. 1 Schematic diagram of a pulse generating linear circuit model. M1, M2 – mirrors, F1, F2 – band-pass spectral filters (transmission bands indicated above), S_p – passive fiber, S_a – active fiber.

Single roundtrip pulse propagation in this circuit was modelled by the following steps:

1. Pulse propagation in L_1 length passive fiber (S_p), modelled by numerical integration of nonlinear Schrödinger equation using Fourier split-step method [23].
2. Pulse amplification in active fiber (S_a). Amplification is described using point amplifier model [24]. Yb-doped fused silica absorption and emission cross-section data provided in [25,26] is used for gain estimation. The excited-state population is calculated using pump power parameter and recalculated after amplification.
3. Pulse propagation in L_2 length passive fiber (S_p), modelled by numerical integration of nonlinear Schrödinger equation.
4. Pulse spectral filtering using band-pass Gaussian filter (F2) centered at λ_{02}. Modeled by Fourier transform of complex amplitude, multiplication by Gaussian distribution filter function (with respect to wavelength) and inverse Fourier transform back to the time domain.
5. Pulse propagation in L_2 length passive fiber (S_p), modelled by numerical integration of nonlinear Schrödinger equation.
6. Pulse amplification using point amplifier model (modelling procedure analogous to step 2).
7. Pulse propagation in L_1 length passive fiber (S_p), modelled by numerical integration of nonlinear Schrödinger equation.
8. Pulse spectral filtering using band-pass Gaussian filter (F1) centered at λ_{01} (modelling procedure analogous to step 4).
9. The cycle is repeated.

In numerical calculations, in the beginning, some initial pulses were used to trigger pulse generation cycle. Next, it was discovered that pulse generation could be triggered by using an initial array of random irradiance values (irradiance noise).

For a broad range of pulse generator circuit parameters, the influence of chromatic dispersion is low and can be neglected. In such cases, the model of pulse generator circuit can be greatly simplified by using analytical expression of SPM effect instead of numerical integration of nonlinear Schrödinger equation. Chromatic dispersion influence is low when narrowband filters and short fiber lengths are used. More precisely, fiber length should be much shorter than dispersion length for pulses with bandwidth relevant to filter bandwidth. Corresponding parameter space when fiber length is ≥10 times shorter than dispersion length is illustrated in Fig. 2.
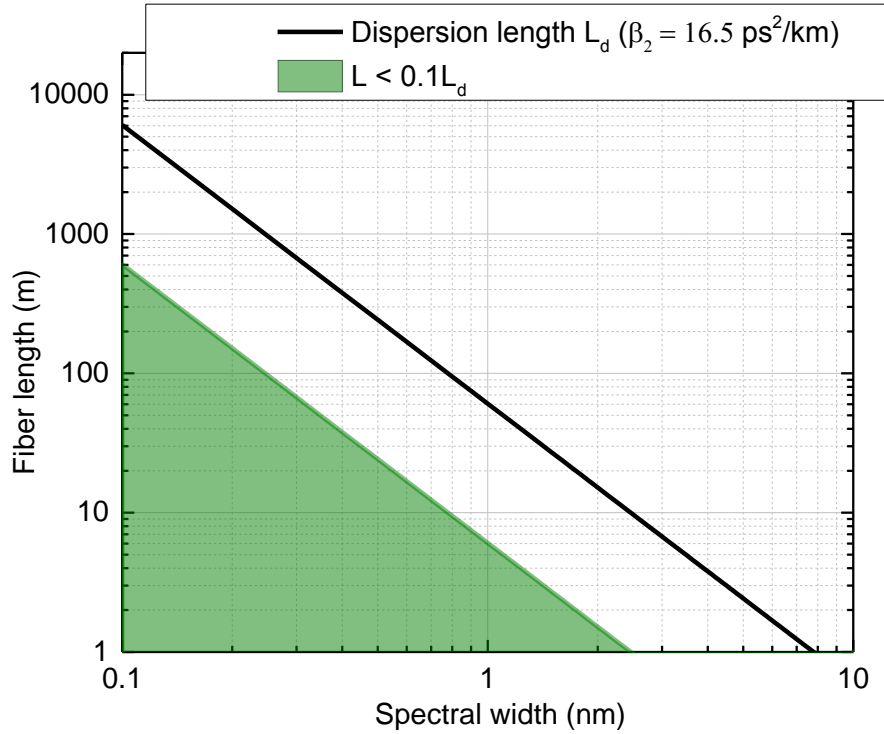
Fig. 2 Dispersion length versus spectral width (FWHM) for Gaussian pulses. Green area corresponds cases when fiber length is ≥10 times shorter than dispersion length. In this calculation fused silica group velocity dispersion parameter was used: $\beta_2 = 16.5 \ \text{ps}^2/\text{km}$.

Moreover, when narrowband filters are used, pulse amplification in fiber can be simplified to wavelength independent gain parameter. Additional simplification can be applied by setting gain parameter constant in time, which is the case during steady-state pulse generation. With these simplifications, numerical calculations can be greatly accelerated, and this allows for analysis of generated pulse characteristics with great variation of circuit parameters. Main parameters which govern pulse characteristics are:

1. Spectral separation of filter bands: $\Delta\lambda_{ats} = \lambda_{02} - \lambda_{01}$
2. Filter spectral bandwidth (FWHM with respect to irradiance): $\Delta\lambda_{f1/2}$
3. Fiber lengths: $L_{1/2}$
4. Gain coefficient: G

To describe the spectral separation of filter bands independently of filter bandwidth, spectral separation parameter S normalized to filter bandwidth is introduced. Also, conducted analysis is restricted to Gaussian filter spectral band distribution and equal filter spectral bandwidths $\Delta\lambda_{f1} = \Delta\lambda_{f2}$.

The main analysis of the described model and influence of circuit parameters for generated pulses was conducted in the case without chromatic dispersion, and then additional effects caused by including chromatic dispersion were indicated. In this summary, results of the numerical analysis are briefly discussed bellow:

- Numerical analysis showed that filter spectral separation parameter governs required pulse spectral broadening, accumulated phase shift, pulse peak power and, accordingly, pulse energy. With the increase of S parameter pulse peak power and energy increases

16

almost linearly. In contrast, pulse duration only slightly depends on filter spectral separation and decreases with the increase of S parameter.

- Filter spectral bandwidth has a major influence on pulse duration. At fixed other parameters, the pulse duration is inversely proportional to filter bandwidth expressed in frequency units. Absolute pulse duration value is slightly higher than duration of bandwidth-limited Gaussian pulses with a spectral bandwidth equal to filter bandwidth. Filter bandwidth also influences pulse energy. More precisely, pulse energy is inversely proportional to filter bandwidth expressed in frequency units.

- Fiber length parameter influences pulse peak power and energy. When both fiber lengths are equal ($L_1 = L_2$), output pulse energy to both outputs is almost equal and inversely proportional to total fiber length. When $L_1 \neq L_2$, parameter space of stable pulse generation is modified, new operation regimes at higher gain values appear. These additional operation regimes correspond to highly non-symmetrical operation with different spectral broadening and pulse energies before outputs 1 and 2.

- Pulse amplification described by gain parameter G is needed to compensate for energy losses caused by spectral filtering and directing part of radiation to the output ports. Numerical calculations showed that stable pulse generation is achieved when the gain parameter value is within some interval. This interval becomes narrower, and average gain value increases with the increase of spectral filter separation parameter S.

- Numerical analysis when chromatic dispersion was included showed that chromatic dispersion has influence not only on the pulse duration but also on gain interval corresponding to the stable pulse generation. With the increase of chromatic dispersion (by increasing fiber length) gain interval of the stable pulse generation broadens significantly. Also, pulse energy characteristics into output 1 and 2 become almost equal through all gain interval corresponding to the stable operation, in contrast to the case without chromatic dispersion. Parameter space of the stable pulse generation, in this operation regime, also depends on spectral separation of filter bands. With the increase of S parameter, broadening of stable operation gain interval shifts to longer fiber lengths. Chromatic dispersion influence on pulse energy is low when fiber length is below dispersion length. However, when fiber length exceeds dispersion length, pulse energy dependence on fiber length departs from dependence described in the model without chromatic dispersion. Pulse energy starts to increase with the increase of fiber length, in contrast to the case without chromatic dispersion.

To verify results provided by numerical analysis, series of experiments were conducted by investigating two fiber generator circuits (Fig. 3). In the first circuit, narrowband fiber Bragg gratings (FBG) were used as Gaussian filters (Fig. 3a). Experiments were conducted using two sets of FBG's with different bandwidth: 0.08 nm and 0.04 nm. In the second circuit, broadband free-space interference filters were used (bandwidth: ~3.5 nm) (Fig. 3b). In both circuits Yb-doped single-mode polarization maintaining fibers were used as a gain medium, wavelength-division multiplexers (WDM) were used for pumping, and some polarizing elements were used for stabilization of state of polarization. The first setup corresponds to pulse generation operation almost without chromatic dispersion influence, and in the second setup, chromatic dispersion effects could not be neglected. Filter spectral band separation was tuned by temperature control of FBG in the first setup and by changing the angle of incidence upon free-space filter in the second setup.

17
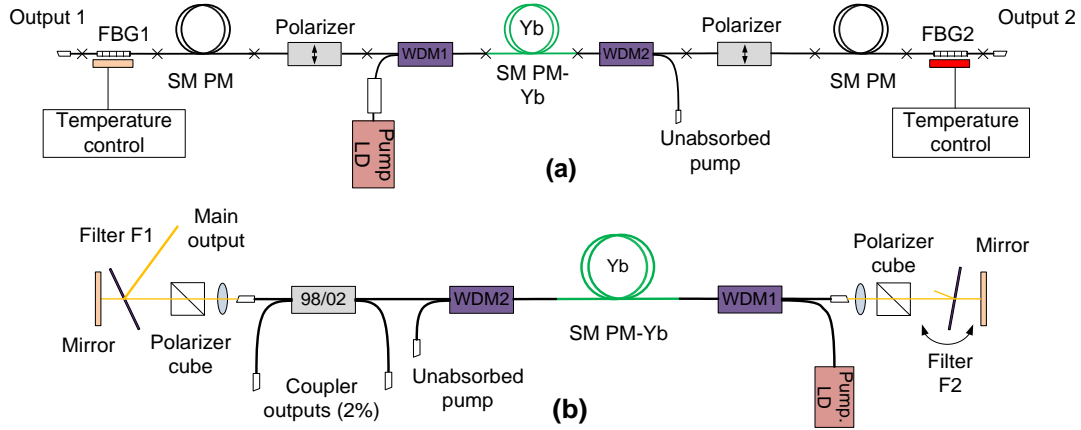
Fig. 3 Schematic diagram of the experimental pulse generator setup with narrowband FBG filters (a) and with free-space interference filters (b).

In the beginning, pulses from the external source were used to excite pulse generation in the experimental setups. Later, it was discovered that self-starting operation is possible when slight overlap between filter bands is set or some additional feedback through output port is organized.

Experimental investigation of the first setup (Fig. 3a) showed that stable pulse generation could be sustained when pump power (and achieved gain accordingly) is tuned slightly (Fig. 4a). This tuning interval was narrow, and pulse generation ceased when pump power was tuned outside the optimal interval.

As it was predicted by numerical modelling, pulse energy increased when fiber length was decreased (Fig. 4b). However, it was increasingly difficult to excite pulse generation when short fiber lengths were used, and so data point corresponding to 34 m total fiber length was measured when external pulse source was used to excite pulse generation in the circuit. Nevertheless, measured pulse energy values support well results of numerical calculations.
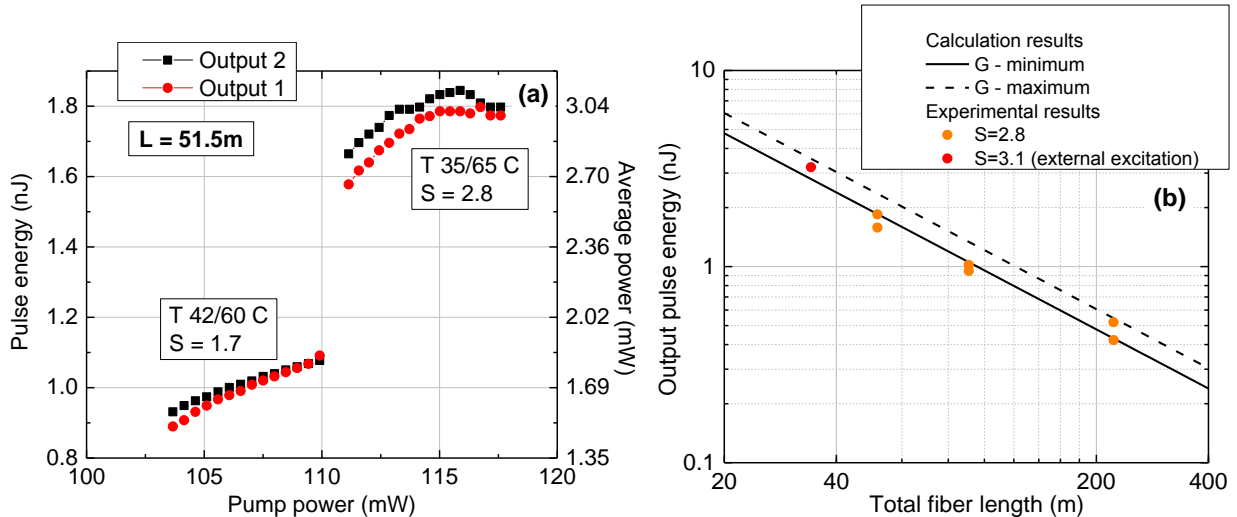
Fig. 4 a) Pulse energy and average power versus pump power, when stable pulse generation is achieved. The total fiber length of the circuit is $L = 51.5$ m. Two groups of data points correspond to different values of spectral filter separation S. b) Output pulse energy versus total fiber length of the circuit. Comparison of experimental data (points) and numerical calculation results (lines). In the calculations, parameters of experimental FBG filters were used (peak transmittance).

Effects of increasing filter band spectral separation were studied by exciting pulse generation at small filter spectral band separation and increasing it afterwards. When S

parameter was increased, usually pump (and accordingly gain) had to be slightly increased to sustain pulse generation. Experimentally measured data compared with numerical calculations is shown in Fig. 5. Despite pulse generation ceased easily when filter band spectral separation was increased too much, measured results agree well with calculated results.
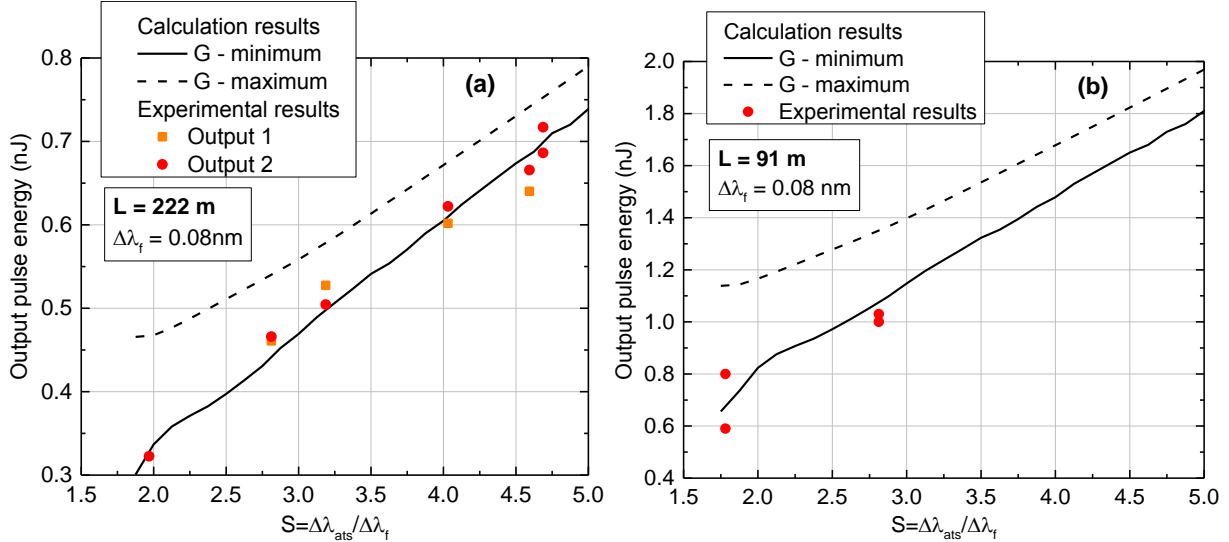
Fig. 5 Output pulse energy versus filter band spectral separation S for two total fiber length values: a) $L = 222$ m; b) $L = 91$ m. Comparison of experimental data (points) and numerical calculation results (lines).

Measured pulse spectra showed generally good agreement with calculated spectra. Pulse duration dependence on filter bandwidth in the first setup was investigated by using two sets of FBG's with different bandwidth, so only two experimental data points were measured (Fig. 6). Nevertheless, measured pulse duration dependence on filter bandwidth is compatible with calculated results.
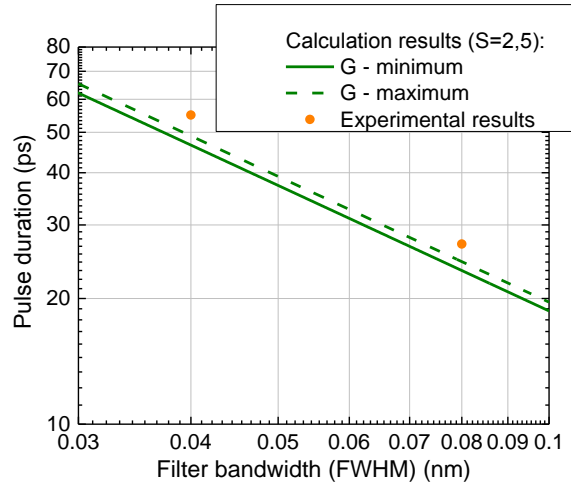
Fig. 6 Pulse duration of generated pulses versus filter spectral bandwidth. Experimental points and numerically calculated lines.

Additionally, pulse compression experiments (for setup with 0.08 nm bandwidth FBG filters) were conducted, and pulse duration of ~4 ps was achieved after compression.

In the second pulse generator setup (Fig. 3b), the operation was greatly influenced by normal chromatic dispersion. Fiber circuit parameters of this setup were mostly fixed (total fiber length was ~8.6 m). By measuring radio frequency spectrum of generated pulse train, it was estimated (using methodology described in [27]) that generated pulses are stable,

with pulse energy fluctuations <0.23 %. Measurements of pulse energy dependence on pump power showed two broad intervals of pump power when stable generation could be achieved (stability zones) (Fig. 7). These two operation intervals also corresponded to different generated pulse spectra.
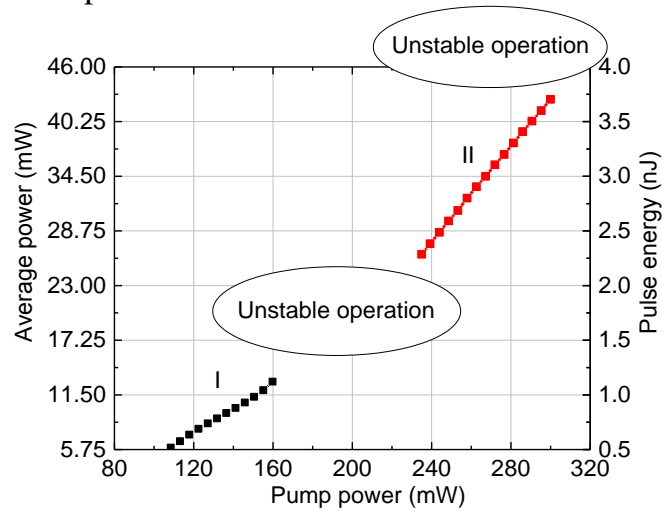
Fig. 7 Pulse energy and average power at main output versus pump power.

Measured pulse energy at lowest pump value (0.52 nJ) was compatible with pulse energy predicted by numerical calculations using full model (0.67 nJ). However, experimental pulse duration was slightly lower than calculated (Fig. 8a). Also, some difference between measured and calculated spectra could be seen (Fig. 8b).
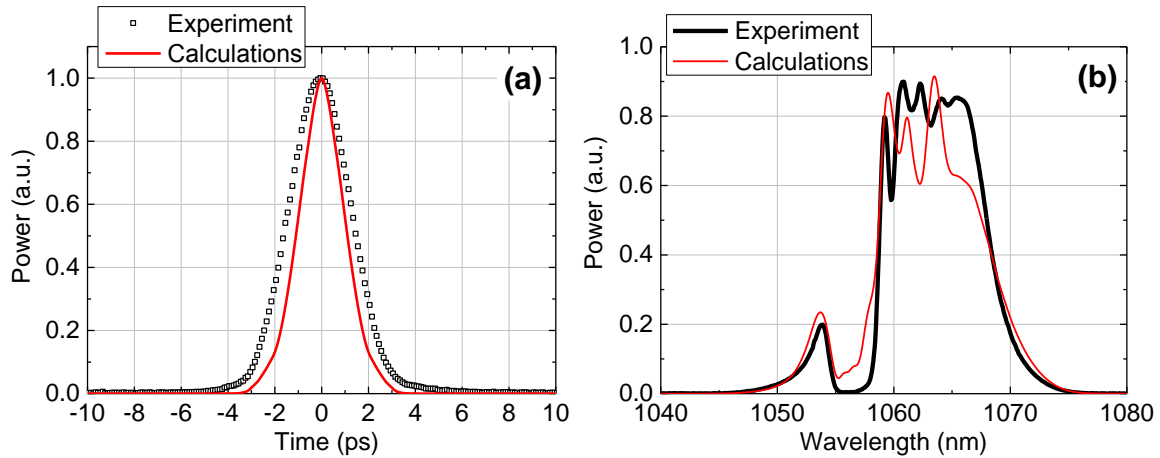
Fig. 8 Comparison of experimental pulse autocorrelation and pulse spectrum at main output with modelling results using full model.

Numerical modelling predicted that generated pulses are chirped and could be compressed. Experimentally pulse compression was accomplished by using diffraction grating compressor with 1000 mm^{-1} line density transmission gratings. When operating in the stability zone I (see Fig. 7), pulses with 228 fs duration and slight pedestal (Fig. 9a) were achieved after compression. When operating in the stability zone II, pulse duration after compression was lower – 145 fs, but unwanted pedestal was bigger (Fig. 9b).

Overall, stable ultrashort pulses with <300 fs duration and high energy of 0.5–3.75 nJ were achieved by using pulse generator setup with broadband filters and high normal dispersion influence. Because of higher pulse energy and broader stability zone with respect to pump (gain), this pulse generator setup seems to be more perspective than the setup without dispersion influence.

20
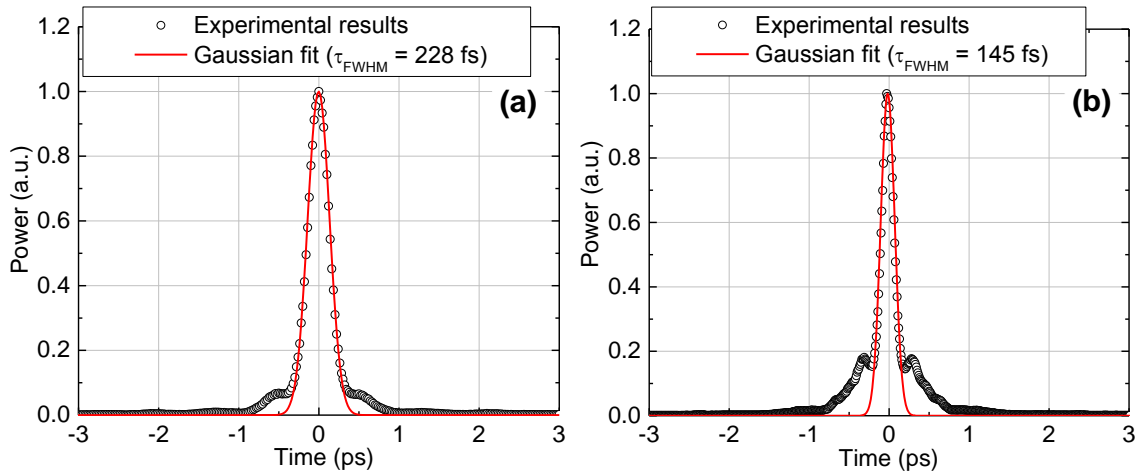
Fig. 9 Autocorrelations of compressed pulses (points) and Gaussian fit functions (red line): a) Operating in the stability zone I (P_{pump} = 136 mW), b) Operating in the stability zone II (P_{pump} = 253 mW).

Chapter 3: Research on optimization of fiber chirped pulse amplification systems

In this chapter, ultrashort pulse amplification in fiber amplifiers by using chirped pulse amplification method is investigated. Nonlinear fiber chirped pulse amplification (FCPA) system is presented in which SPM is utilized both in pulse stretcher and main amplification stages. Schematic diagram of the investigated FCPA setup is depicted in Fig. 10.
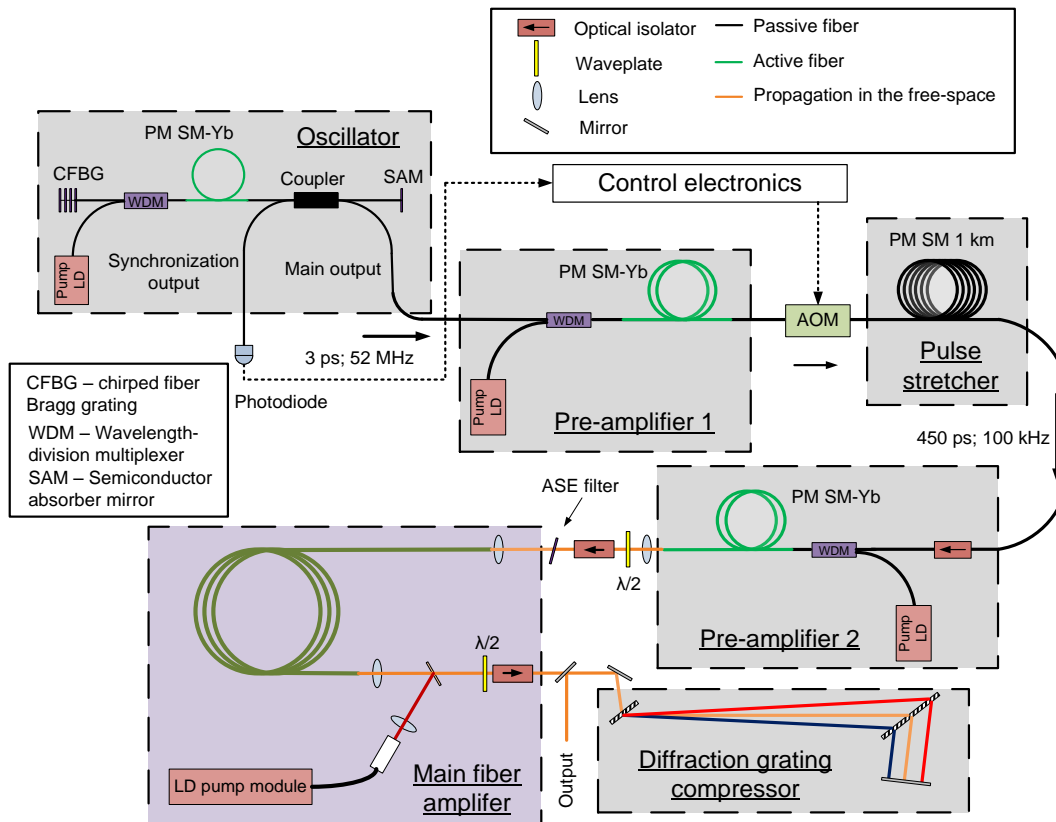
Fig. 10 Schematic diagram of the experimental FCPA setup.

The system was seeded by passively mode-locked fiber oscillator, which generated bandwidth-limited pulses with 3.2 ps duration (FWHM) at 1064,7 nm central wavelength. These pulses were amplified in the first pre-amplifier based on single-mode (SM)

polarization maintaining (PM) Yb-doped core-pumped fiber. In this amplification stage, pulse energy was increased up to a level sufficient to achieve required spectral broadening in the fiber stretcher. Then, acousto-optic pulse-picker was used to reduce pulse repetition rate down to 100 kHz.

Pulse stretcher stage consisted of 1 km-length SM PM fiber. In this stage, pulses were stretched both in spectral and time domains because of combined effects of SPM and normal chromatic dispersion. This allowed achieving triangularly-shaped highly-chirped pulses which could be compressed down to a duration shorter than the duration of pulses from the fiber oscillator. Pulse energy at the input of the fiber stretcher was optimized according to required pulse spectral and temporal broadening. After optimization, pulse energy value of ~1.6 nJ was selected and this allowed to achieve stretched pulses with ~450 ps duration (FWHM) and ~11 nm bandwidth (Fig. 11). Experimental pulse spectrum exhibited high-frequency modulation at its peak (Fig. 11b). This modulation was caused by interference between the spectrum of the stretched pulses and spectral side-bands which are a characteristic feature of oscillators operating in soliton pulse regime, like the one used in this work. Spectral side-bands of the oscillator pulses were registered experimentally and were reproduced by using numerical modelling. The spectrum of the stretched pulses also showed some deviation from triangular shape at its peak (Fig. 11b). This was caused by limited contrast ration of AOM (~40 dB). High-repetition-rate pulses from the oscillator were highly attenuated, but being more numerous (52 MHz versus 100 kHz), still represented 9 % of total average power. This was confirmed by modelling results including the contribution of low-energy high-repetition-rate pulses (Fig. 11b). Pulse propagation in the fiber stretcher was modelled by numerical integration of nonlinear Schrödinger equation using Fourier split-step method [23]. Nonlinear refractive index and dispersion parameters used in modelling were $n_2 = 2.6 \cdot 10^{-20}$ m^2/W and $\beta_2 = 2.3 \cdot 10^{-2}$ ps^2/m, $\beta_3 = 4.6 \cdot 10^{-5}$ ps^3/m respectively. Results of numerical modelling are presented together with experimental results in Fig. 11. Numerical modelling also showed that stretched pulses are mostly linearly chirped and could be compressed down to ~300 fs duration by inducing required amount of GVD and TOD.
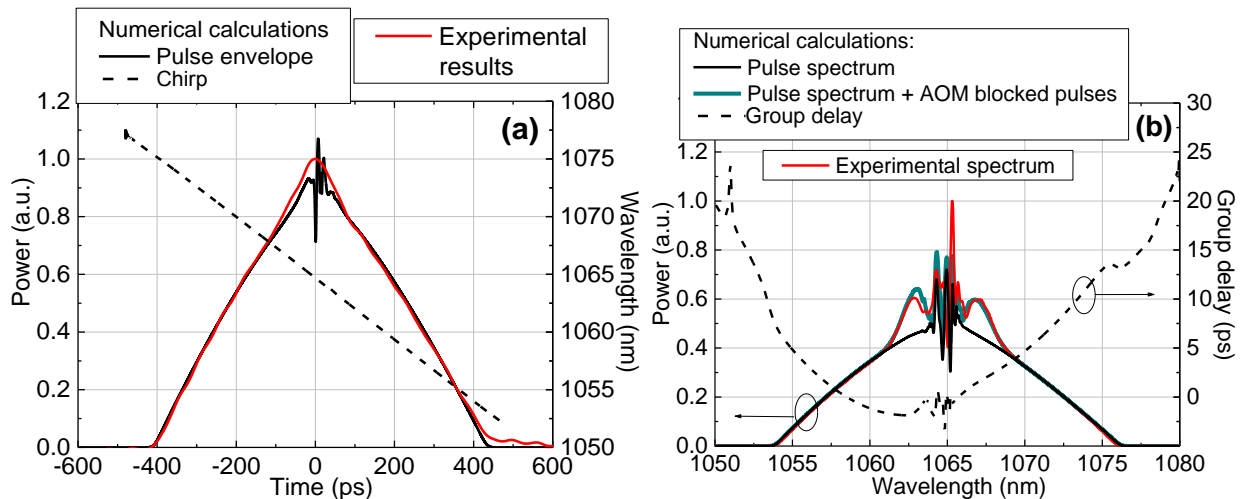
Fig. 11 a) Temporal envelope of the stretched pulses (red – experimental results, black – numerical calculations) and chirp of numerically calculated pulses (dashed line). b) The spectrum of the stretched pulses (red – experimental results, black – numerical results, blue – numerical results with the inclusion of contribution of AOM blocked pulses) and calculated spectral group delay curve after linear part (caused by GVD) was numerically compensated (dashed line).

22

Stretched pulses were amplified in the second fiber pre-amplifier analogous to the first one (Fig. 10). In this stage, pulse energy was increased up to an optimal value for amplification in the main fiber amplifier stage. Experiments were conducted using three fibers with different core sizes in the main amplification stage. Two of them were conventional large mode area (LMA) double-clad (DC) PM fibers, and one was experimental chirally-coupled-core (CCC) DC fiber. Parameters of these fibers are presented in Table 1.

Table 1 Parameters of the fibers used in the main amplification stage.

	12 µm core diameter fiber	25 µm core diameter fiber	CCC fiber
Model No	Yb1200-12/125DC-PM	Yb1200-25/250DC-PM	
Core diameter:	12.5 µm	25.5-26.4 µm	33 µm
Effective mode diameter (area) (1064 nm):	12.6 µm (125 µm^2)	21.3 (356 µm^2)	27 µm (573 µm^2)
Core numerical aperture:	0.084	0.070-0.077	-
Polarization maintaining:	Yes (PANDA)	Yes (PANDA)	Yes
Birefringence:	$1.4 \cdot 10^{-4}$	$1.4 \cdot 10^{-4}$-$2 \cdot 10^{-4}$	-
Pumping region:	Internal cladding	Internal cladding	Internal cladding
Diameter of internal cladding:	125 µm (circular)	249 µm (circular)	257 µm (circular)
Cladding pump absorption (920 nm):	3.1 dB/m	2.7-2.8 dB/m	3.2–3.8 (915 nm)
Estimated saturation energy (1064 nm):	74 µJ	210 µJ	338 µJ

For pumping of the main fiber amplifier, both counter-propagating and co-propagating pumping configurations were investigated. First one was shown in Fig. 10. In the second configuration, pump and signal combiner component was spliced to the input of active fiber (Fig. 12).
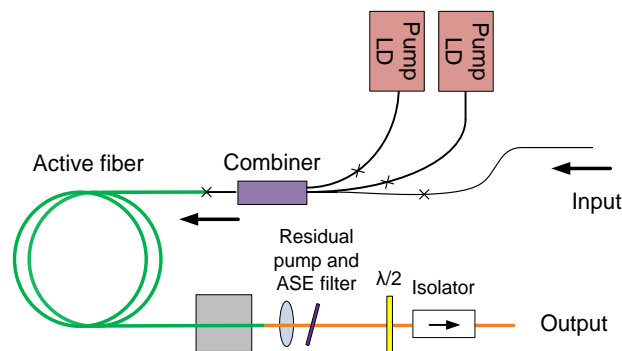
Fig. 12 Schematic diagram of the main amplification stage organized in co-propagating pumping configuration by using pump and signal combiner.

Experimental investigation of the described FCPA system showed that using counter-propagating pumping configuration, the threshold of nonlinear effects can be tuned by changing input pulse energy and gain in the main fiber amplifier. This is related to the effective length of active fiber which depends on achieved gain [23]. Detailed

experimental analysis of stimulated Raman scattering (SRS) threshold dependence on input pulse energy was carried out in the setup with 12 μm core diameter fiber (length: 2.4 m) at the main amplification stage. Results showed that by reducing input pulse energy from 130 nJ to 30 nJ and increasing gain (by increasing pump power), output pulse energy, corresponding to the fixed level of SRS (Fig. 13b), could be increased by 30 % (Fig. 13a). Reduction of input pulse energy below 30 nJ was limited by the onset of amplified spontaneous emission (ASE) in the spectral region of the highest gain (~1030 nm).
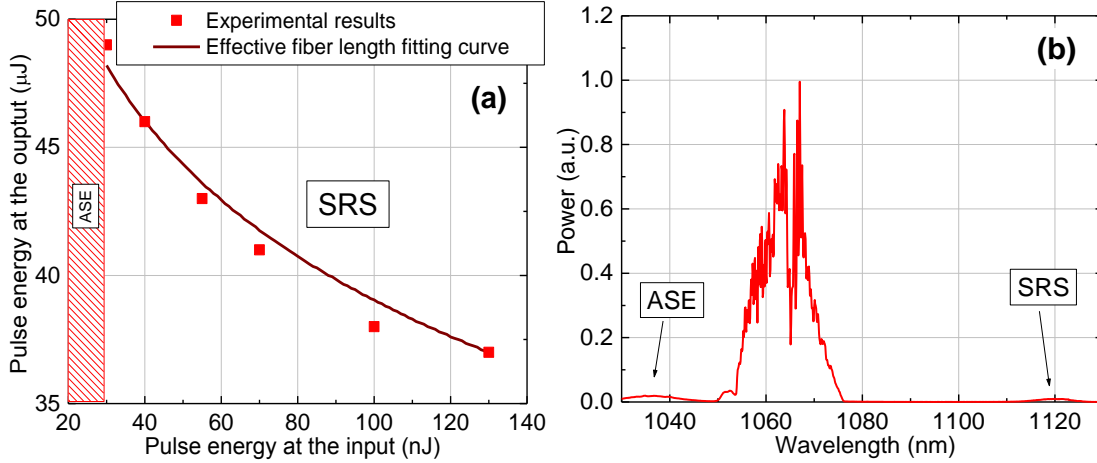
Fig. 13 a) Achievable output pulse energy (corresponding to fixed level of SRS) versus input pulse energy: experimental results (points) and fitting curve based on effective fiber length expression. b) The spectrum of the stretched pulses amplified to 48 μJ, when input pulse energy is 30 nJ.

In contrast, when using co-propagating pump configuration, nonlinear-effect-limited output pulse energy was almost independent on input pulse energy. Thus, to increase the threshold of detrimental nonlinear effects, fiber length had to be tuned precisely. Detailed experimental investigation of the influence of the fiber length for achieved maximum pulse energy (before nonlinear effects appear) was carried out in the setup with 25 μm core diameter main fiber amplifier pumped through pump and signal combiner. Achieved amplified pulse energy and limiting nonlinear effects are summarized in Table 2. For fiber lengths ≥1.6 m, pulse energy was mostly limited by the generation of new spectral components which is an indication of four-wave mixing (FWM) effect. On the other hand, for fiber lengths ≤0.7 m, pulse amplification was limited by achievable gain.

Table 2 Pulse amplification results using different lengths of 25 μm core diameter active fiber.

Length of active fiber (m)	Achieved maximum pulse energy (μJ)	Limiting effects
2.4	35	SRS, generation of new spectral components at wavelengths of ~1500 nm and ~675 nm
1.6	47	Generation of new spectral components at wavelengths of ~1500 nm and ~675 nm
1.2	80	-
0.7	33	Achievable gain

The amplified pulses were compressed using conventional Treacy-type diffraction grating compressor [28] with high-efficiency transmission diffraction gratings (groove

density: 1000 mm^{-1}). Optimal pulse compression was achieved when the distance between gratings was 3,6-3,8 m. Pulse compression experiments were conducted for pulses amplified in all three main amplifier fibers. However, in this summary pulse compression of pulses amplified only in CCC fiber will be discussed in more detail.

Using CCC fiber (~2 m) in counter-propagating pumping scheme for the main amplifier, stretched pulses were amplified up to 100 μJ pulse energy (10 W average power). The achievable pulse energy was limited by degradation of polarization extinction ratio (PER) (Fig. 14b) and spectral distortions (modulation). No signs of other nonlinear effects were registered in the pulse spectrum (Fig. 14a).
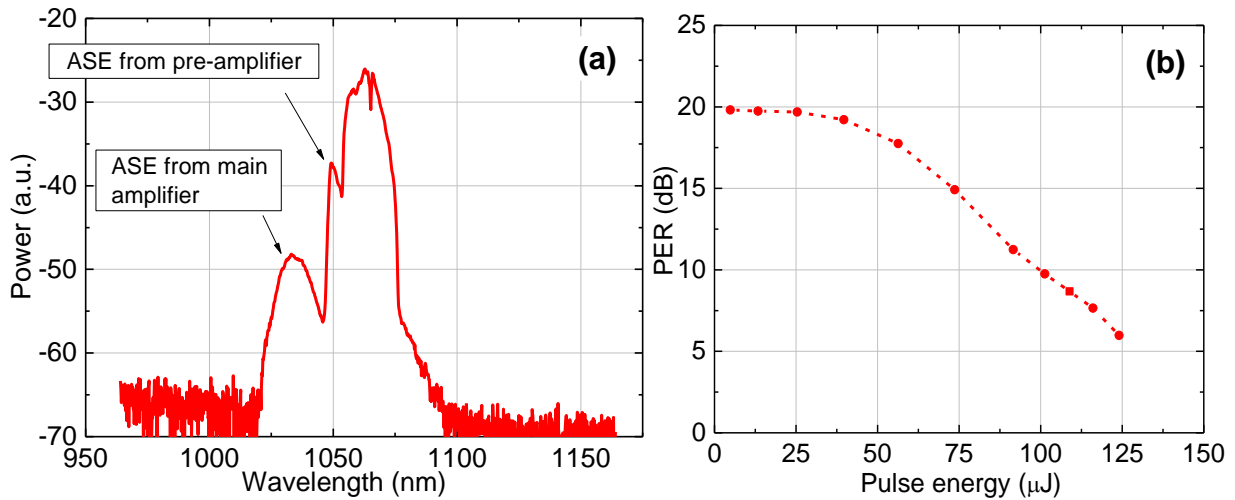
Fig. 14 a) Spectrum of the amplified pulses from the CCC fiber amplifier. b) PER versus output pulse energy at the output of the CCC fiber amplifier.

Amplified stretched pulses exhibited non-symmetrical envelope in time and spectral domain (Fig. 15). Such behavior was caused by gain shaping in a Yb-doped fiber amplifier and was also present for all tested fibers. SPM influence for such non-symmetrical pulses generates nonlinear phase which is opposite to positive TOD induced by diffraction grating compressor. This allows for better compression of amplified pulses. Such effect was confirmed by numerical modelling based on numerical integration of nonlinear Schrödinger equation with included wavelength-dependent gain.
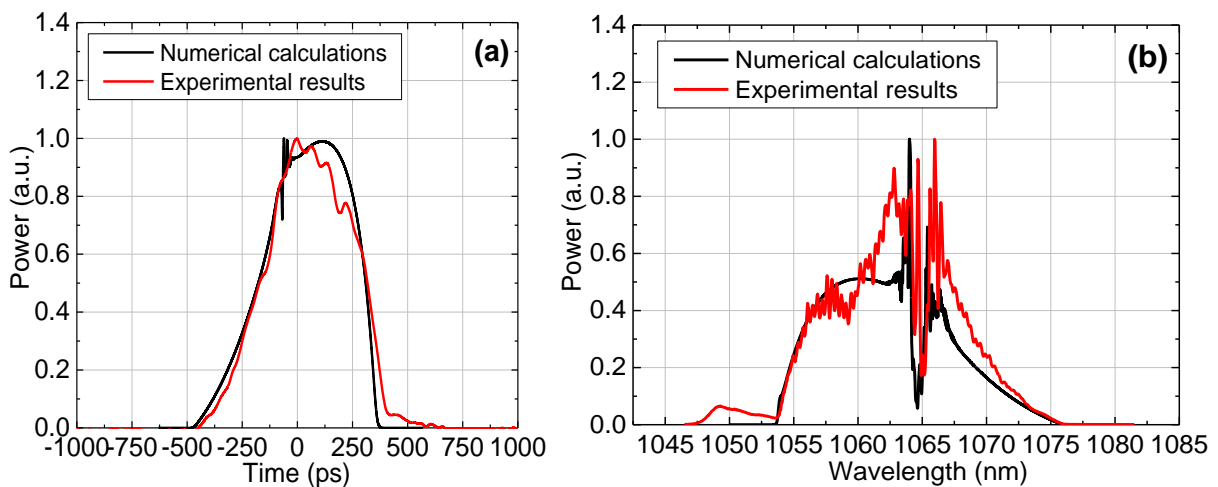
Fig. 15 a) Temporal envelope of the amplified pulses from the CCC fiber amplifier (red – experimental results, black – numerical results). The spectrum of the amplified pulses (red – experimental results, black – numerical results).

25

Experimental results showed that 400 fs duration pulses could be achieved after compression when part of the pulse spectrum is filtered in the compressor (Fig. 16a). Also, experimental results confirmed that by increasing output pulse energy (and SPM induced nonlinear phase), pulse compression improves (Fig. 16b). This demonstrates that SPM influence for chirped non-symmetrical pulses in fiber amplifier is indeed beneficial for pulse compression. After compression, pulses with 50 µJ energy were achieved, and output beam quality was nearly diffraction-limited with $M^2 = 1,1$.
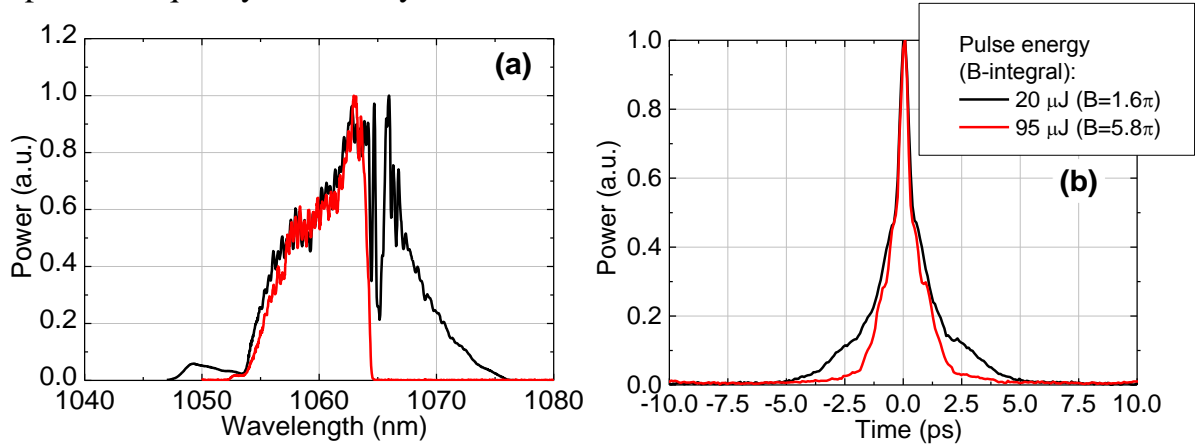
Fig. 16 a) Pulse spectrum at the output of the CCC fiber amplifier (black) and pulse spectrum after spectral filtering in the compressor (red). b) Autocorrelation of the compressed pulses at 20 µJ (black) and 95 µJ (red) output pulse energy.

Achieved pulse amplification and compression results using other fibers in the main amplifier are compared and summarized in Table 3. In all investigated cases, pulses with a duration of <450 fs were achieved after compression. This is >7 times shorter pulse duration than the duration of initial pulses provided by the oscillator.

Table 3 Summarized pulse amplification and compression results using different main fiber amplifier configurations.

Main amplifier	Pumping configuration	Maximum pulse energy (peak power) after amplification	Pulse energy limiting effect	Optimal pulse energy from amplifier for compression (µJ)	B-integral (rad)	Pulse duration after compression (fs)	Pulse energy after compression (µJ)
12 µm fiber amplifier	Counter-propagating	48 µJ (107kW)	SRS	35	10,3π	360	17
	Co-propagating	28 µJ (62kW)	Achievable gain	23		450	8
25 µm fiber amplifier	Counter-propagating	90 µJ (200kW)	FWM	73	8,8π	370	30
	Co-propagating	80 µJ (178kW)	-	-		-	-
CCC fiber amplifier	Counter-propagating	100 µJ (222kW)	PER degradation	100	6.1π	400	50

Highest achieved pulse energy after compression was compared between all tested fibers operated in counter-propagating pumping configuration (Fig. 17). Such comparison indicates that highest pulse energy per mode area was achieved using 12 µm core diameter active fiber. This can be attributed to better suppression of nonlinear effects in 12 µm core diameter fiber. In this fiber, achievable pulse energy was limited by SRS effect, and in 25 µm core diameter fiber, FWM was registered first. It is known that FWM threshold is lower by a factor of ~2 than SRS threshold [23]. However, FWM process is efficient only when phase-matching conditions are fulfilled for interacting waves. Usually, it is not the case, but phase matching can be achieved through higher-order modes propagating in the fiber. 12 µm core diameter fiber is almost single-mode with only one leaky higher-order mode possible. However, in 25 µm core diameter LMA fiber, which was used in this work, 5 higher-order modes can be supported (according to calculations). This can explain why in 25 µm core diameter fiber, maximum pulse energy was limited by FWM process and in 12 µm core diameter fiber, pulse energy could be increased up to SRS threshold.
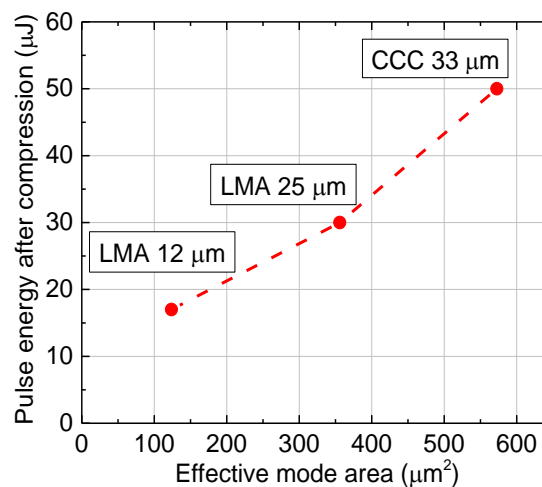
Fig. 17 Experimentally achieved pulse energy after compression versus effective mode area.

Using CCC fiber neither FWM nor SRS effects were registered, and maximum pulse energy was limited by some nonlinear PER degradation. This behavior is probably related to operation peculiarities of CCC technology fiber.

In Table 3 roughly estimated SPM induced nonlinear phase (B-integral) is indicated as well. All fiber amplifiers operated in the nonlinear regime and highest estimated B-integral value was achieved using 12 µm core diameter active fiber.

Chapter 4: Second harmonic generation of broadband radiation from fiber lasers by inducing temperature gradient along a nonlinear crystal

In this chapter, method for second harmonic generation (SHG) of broadband (chirped) pulses from fiber lasers is presented and investigated both numerically and experimentally. Discussed method is based on the dependence of phase-matching wavelength on the temperature in birefringent nonlinear crystals and was first theoretically described in R. Haas work [29]. By setting constant temperature gradient along nonlinear crystal, phase-matching conditions at different parts along the crystal are fulfilled for different spectral components of the broadband radiation. This allows to generate the second harmonic of the broadband radiation in longer crystals (than using conventional SHG configuration)

and achieve higher conversion efficiency. In this chapter, such method is investigated by utilizing temperature tuning capabilities of LiB_3O_5 (LBO) nonlinear crystal cut normal to x-axis. In such configuration, type I non-critical phase matching in LBO crystal can be achieved at wavelength region around 1064 nm (Fig. 18), which features the absence of walk-off and very wide acceptance angle.
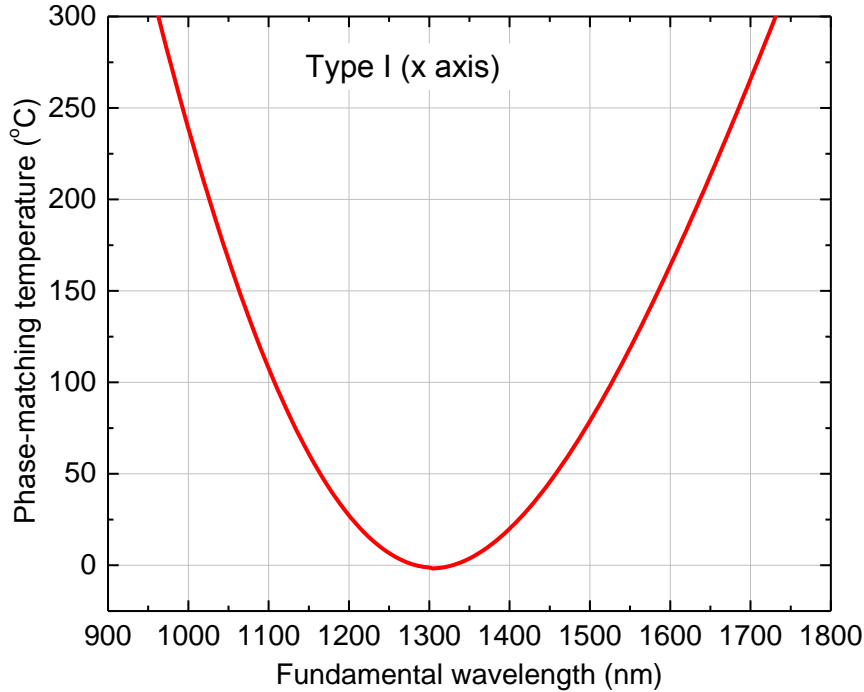
Fig. 18 Phase-matching temperature dependence on fundamental wavelength for propagation direction along x-axis of LBO crystal ($\theta=90°$, $\varphi=0°$). [30]

First, numerical modelling of SHG in the LBO crystal both with and without temperature gradient was accomplished. The nonlinear interaction was modelled by numerical integration of coupled-wave equations using the split-step technique in which propagation is handled by Fourier transform methods, whereas nonlinear interaction is handled by Runge–Kutta integration [31,32]. Temperature influence was included by using temperature dependent expressions of refractive index [30]. The analysis was restricted to SHG of linearly chirped Gaussian pulses with spectral bandwidth controlled by selecting chirp parameter.

Numerical analysis showed that in the case when crystal temperature was uniform (corresponding to phase-matching at center wavelength), crystal length had to be optimized for each spectral bandwidth value to achieve highest conversion efficiency. Required peak irradiance to achieve adequate conversion efficiency, when crystal length was optimal, is presented in Fig. 19. These results indicate that conversion efficiency is strongly dependent on pulse bandwidth. For example, to maintain constant conversion efficiency after increasing spectral bandwidth N times, peak irradiance should be increased roughly N^2 times. This is valid for pulses with duration >1 ps. For shorter and bandwidth-limited pulses, high conversion efficiency can be achieved in long crystals despite the effects of spectral narrowing and pulse broadening caused by the group-velocity mismatch.
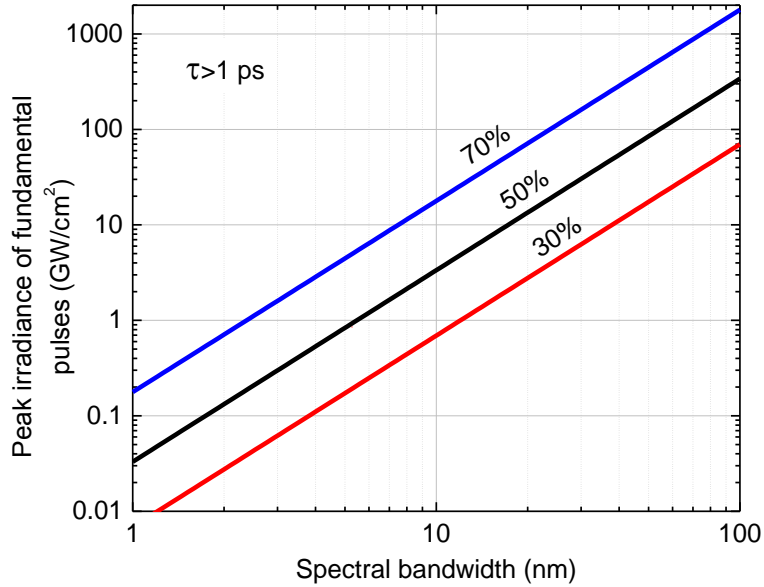
Fig. 19 Peak irradiance of the broadband fundamental pulses required to achieve a conversion efficiency of 30 %, 50 %, 70 %. Temperature along the LBO crystal is uniform, and crystal length is optimized for highest conversion efficiency for each spectral bandwidth value.

Numerical calculations of the temperature gradient influence for SHG conversion efficiency were carried out for 3 cm long crystal and 10 ps duration pulses but are valid for any pulse duration >1 ps. In Fig. 20 conversion efficiency dependence on the temperature gradient value ($\mathrm{d}T/\mathrm{d}z$) is shown for 4 different spectral bandwidth cases. These results demonstrate significant SHG conversion efficiency improvement of the broadband pulses, compared to the case when crystal temperature is constant. For example, to achieve 70 % conversion efficiency, at uniform crystal temperature and for pulse spectral bandwidth of 100 nm, required peak irradiance is 1.79 TW/cm^2 (Fig. 19) which is nearly two orders of magnitude above surface optical damage threshold of the LBO crystal [33,34]. However, when the optimal temperature gradient is imposed along the crystal, 70 % conversion efficiency can be achieved at the peak irradiance of only 10 GW/cm^2. Calculation results also demonstrate that with increasing peak irradiance, temperature gradient should be increased to achieve optimal conversion efficiency. This can be explained by shorter interaction length, needed to achieve the same conversion efficiency for some narrow part of the broadband spectrum. The temperature gradient can be increased by such amount that conversion efficiency for this narrow part of the spectrum stays the same but total range of the converted wavelengths increases. Thus phase-matching for broader spectrum can be achieved, and total conversion efficiency increases. It is evident that total range of wavelengths which can be converted to second harmonic depends on the temperature tuning characteristics of the LBO crystal and temperature difference between crystal endfaces but not on the crystal length. This is contrary to the case when crystal temperature is uniform. Fig. 20 also indicate that when the temperature gradient is higher than optimal, conversion efficiency depends weakly on the temperature gradient. Such feature can be advantageous for SHG of high-average-power broadband radiation. Furthermore, analysis of temporal and spectral envelopes of second harmonic pulses revealed that periodic modulation appears on the temporal and spectral envelope. Amplitude and period of this modulation decrease when the temperature gradient is increased. Also, when the temperature gradient is increased, crystal length should be increased accordingly to maintain the same conversion efficiency.

29
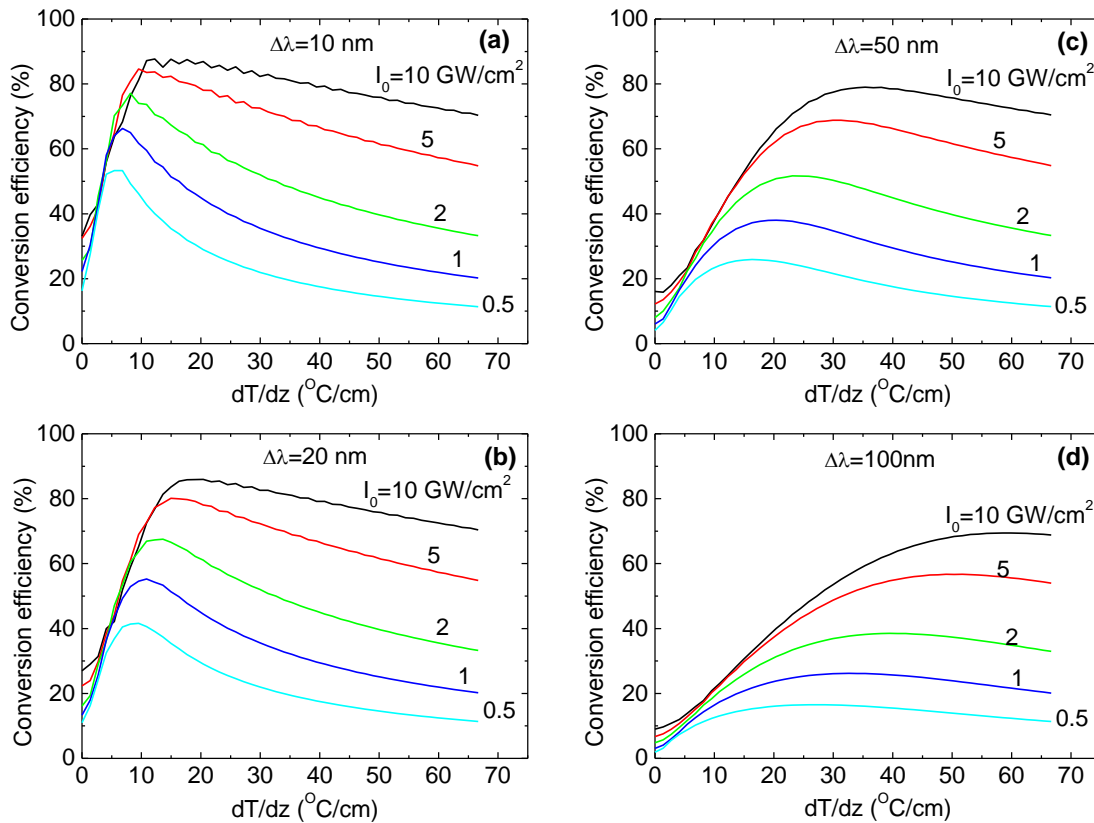
Fig. 20 SHG conversion efficiency dependence on temperature gradient (dT/dz) for various values of the peak irradiances of the broadband fundamental pulses (0.5, 1, 2, 5 and 10 GW/cm^2) and spectral bandwidth: 10 nm (a), 20 nm (b), 50nm (c) and 100 nm (d).

Experimental investigation of SHG in LBO crystal with longitudinal temperature gradient was accomplished using 8 ps duration pulses (1064 nm center wavelength) generated in passively mode-locked fiber oscillator and amplified in CCC main fiber amplifier up to 2.8 µJ pulse energy (Fig. 21). Because of SPM in the fiber amplification stages pulse spectrum was broadened up to ~12 nm.
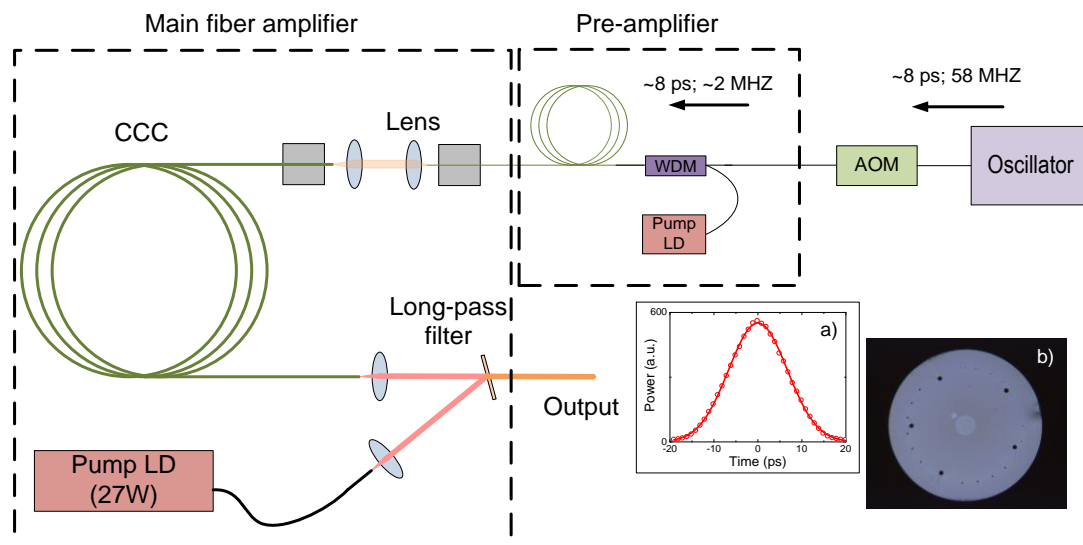
Fig. 21 Schematic diagram of the fiber laser system. Insets: (a) autocorrelation of the amplified pulses, (b) microscopic picture of CCC fiber cleaved endface. AOM – acousto-optic modulator, WDM – wavelength-division multiplexer.

The laser beam from fiber amplifier was focused into the crystal (130 μm waist diameter). LBO crystal with length of 3 cm and mounted in custom designed crystal oven was used for SHG with temperature gradient experiments. Because of group-velocity mismatch, phase-matching bandwidth in the crystal of such length was limited to 1.27 nm (at 1064 nm center wavelength). However, when optimal temperature gradient was set, the whole broad spectrum was converted to the second harmonic (Fig. 22a). Measurements of conversion efficiency also showed significant conversion efficiency improvement compared to the case when the crystal temperature was uniform (Fig. 22b). Additional experiments were carried out using shorter (1 cm) LBO crystal set in critical phase-matching configuration (θ = 90°, φ = 11,6°). In these experiments, the laser beam was sharply focused (50 μm waist diameter) in the crystal to achieve higher irradiance and conversion efficiency. Estimated irradiance in the crystal, in this case, was 25 GW/cm² which is near damage threshold according to some sources [33]. Nevertheless, achieved conversion efficiency was still lower than in the setup with a temperature gradient along nonlinear crystal.
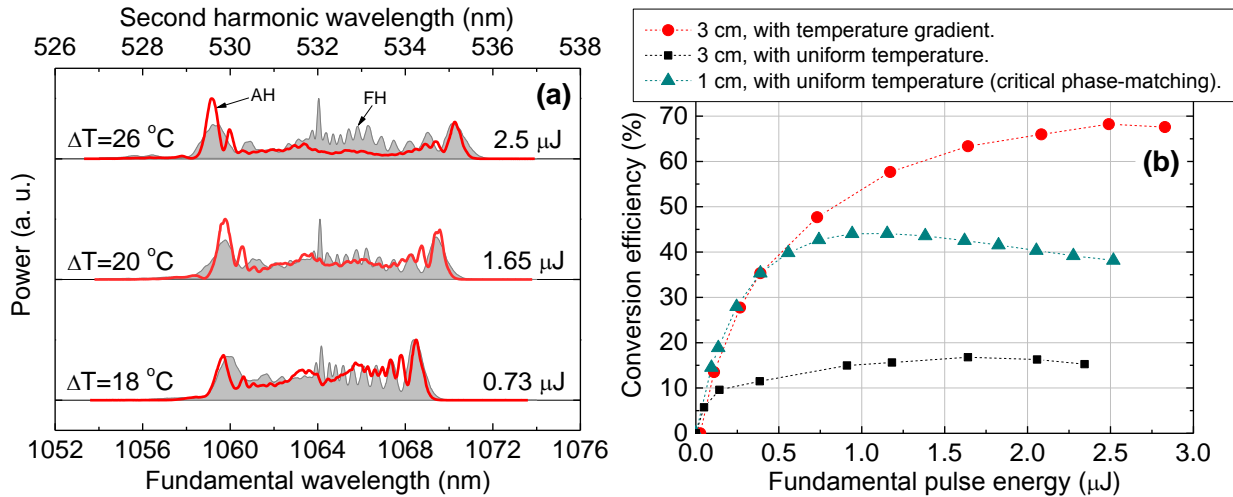
Fig. 22 (a) Comparison of the generated second harmonic spectrum with fundamental spectrum at different fundamental pulse energy (0.73, 1.65 and 2.5 μJ), when the temperature gradient is applied along the crystal. Grey curves with filled regions represent fundamental spectra, and thick red curves represent second harmonic spectra. ΔT – the temperature difference between crystal endfaces. (b) SHG conversion efficiency versus pulse energy in case of 3 cm long crystal with longitudinal temperature gradient (circles), 3 cm long crystal without longitudinal temperature gradient (squares) and 1 cm long crystal in critical phase-matching configuration and without the longitudinal temperature gradient (triangles).

Chapter 5: Nonlinear combining of pulsed beams from fiber lasers

In this chapter, two methods for combining of pulses from fiber lasers, by sum-frequency generation in quadratic susceptibility crystal, are presented and investigated experimentally. The first method allows to combine pulsed laser beams from multiple fiber amplifiers into a single beam, in which pulses are multiplexed in time, and together accomplish optical frequency up-conversion. In such way, pulse repetition rate and average power in the combined beam can be increased. The second method allows combining two separated in time pulses of the same beam into single sum-frequency pulse and achieve higher pulse energy (and peak power) than in conventional SHG configuration. In another implementation of the second method, leading part of the single

long pulse can be combined with trailing part of the same pulse and so pulses with shorter by a factor of 2 duration can be achieved.

Nonlinear beam combining and pulse multiplexing in time

First combining method is based on phase-matching properties of the noncollinear three-wave interaction process. Calculated phase-matching directions of the fundamental beams for the LBO crystal, corresponding to the same sum-frequency beam direction, are shown in Fig. 23. Any pair of fundamental beam directions corresponding to these circles and lying in the same plane as the sum-frequency beam can generate sum-frequency beam in the same direction (direction of the sum-frequency beam). From this it is evident that there are multiple possible directions in which pairs of fundamental beams can be arranged. If pulses of multiple beam pairs do not overlap in time, these pulses can be multiplexed in time into single sum-frequency beam without additional active phase control.
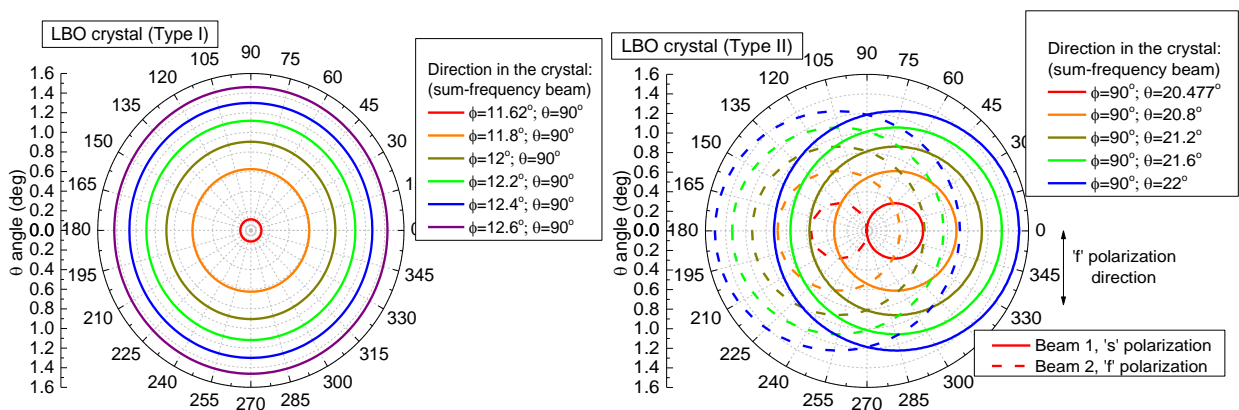
Fig. 23 Calculated angular distribution of the phase-matched fundamental (1064 nm) beam propagation directions in the LBO crystal (Type I and Type II) with respect to the propagation direction of the sum-frequency beam. Different colors refer to the different direction of the sum-frequency beam in the crystal (i.e. crystal orientation). The LBO crystal parameters used in the calculations are described in literature [30].

Experimental investigation of the beam combining and pulse multiplexing in time method was carried out by combining two pairs of pulsed beams from 4 fiber amplifiers into the single (frequency up-converted) beam (refer to Fig. 25b). Two sources of optical pulses operating at 1064 nm center wavelength were used for the experiments (Fig. 24). The first source (A) was a microchip laser which generated 400 ps duration, ~500 nJ energy pulses at 5 kHz repetition rate. The second source (B) consisted of passively mode-locked fiber oscillator, a pair of single-mode Yb-doped pre-amplifier stages and acousto-optic pulse picker in-between. Second pulse source generated 200 ps duration pulses with 33 nJ energy at 512 kHz repetition rate. Pulses from these sources were divided into 4 channels (Fig. 24) and amplified in 4 separate fiber amplifiers based on 25 µm core-diameter LMA DC PM Yd-doped fibers. Mode field adapters were produced for coupling optical pulses into the LMA fibers. Pumping configuration of these fibers was counter-propagating. Pulse amplification experiments showed that pulses from source A could be amplified up to ~100 µJ (0,5 W average power) before the onset of SRS with some signs of FWM and pulses from source B could be amplified up to ~31,3 µJ pulse energy (16 W average power) in each of fiber amplifiers.
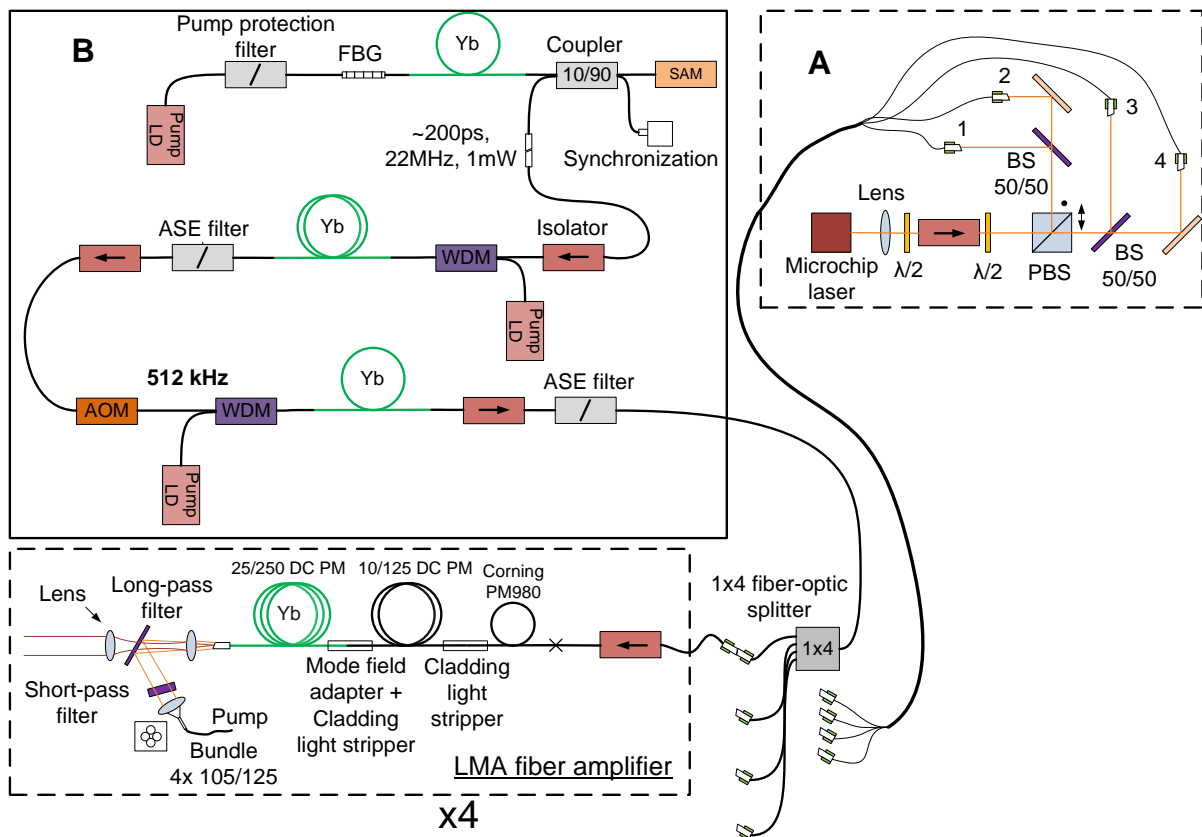
Fig. 24 Schematic diagrams of the optical pulse sources (A, B) and LMA fiber amplifiers. AOM – acousto-optical pulse picker, WDM – wavelength-division multiplexer, SAM – semiconductor absorber mirror, FBG – fiber Bragg grating, BS – beam splitter, PBS – polarizer beam splitter.

Laser beams from 4 fiber amplifier channels were arranged as illustrated in Fig. 25a and focused into the nonlinear crystal. Delay lines were implemented for beams of channels 1 and 4 to fine-tune pulse overlap in time. Pulses from channel 1 should overlap with pulses from channel 3 but pulses from channel 4 should overlap with pulses from channel 2. Pulses of different pairs (channels 1+3 versus channels 2+4) should be separated in time to allow for pulse multiplexing in time. The time delay between pulses of different pairs was set by choosing right fiber lengths between pulse source and inputs to the fiber amplifiers.
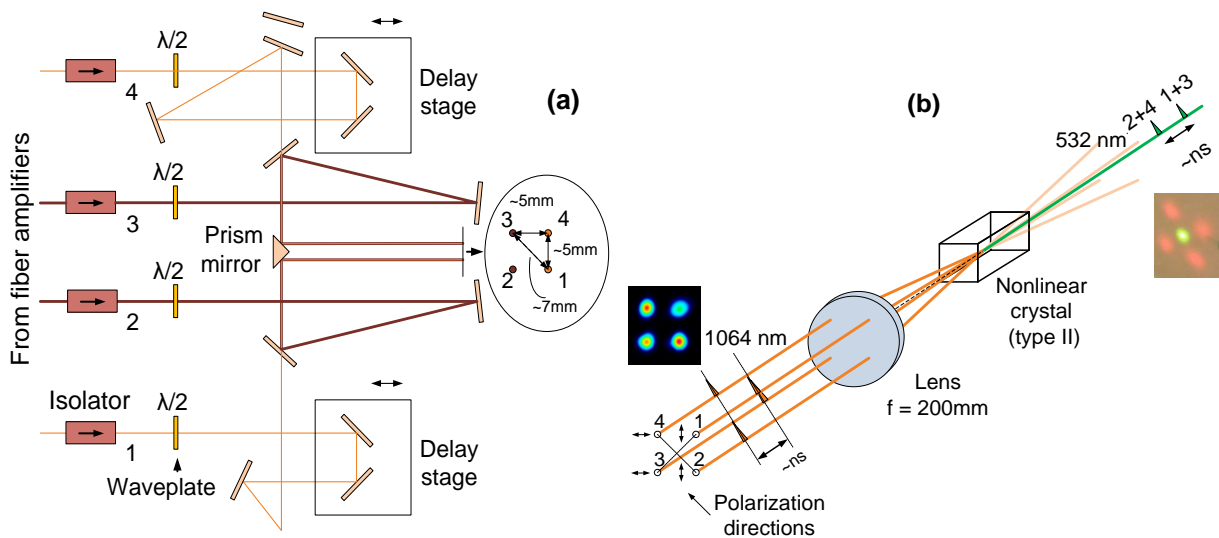
Fig. 25 a) Schematic diagram of the setup (view from above) for arranging and directing all four fundamental beams to the crystal. b) Schematic diagram of the setup for the beam focusing into the crystal.

Beam combining in two different crystals was tested experimentally: KTP (cut angles: θ=90°, φ=~24; lengths: 3 and 8 mm) and LBO (cut angles: θ=21°, φ=90°; length: 20 mm). In experiments with KTP crystal, only amplified pulses from the source A were used because KTP crystal could not withstand high average power achievable when amplifying pulses from source B. In experiments with LBO crystal, both pulse sources were used.

Beams corresponding to four different channels were focused in the crystal using 200 mm focal length lens as it is shown in Fig. 25b. Beam waist diameter was 200 μm with a slight variation of 15% between different channels. The intersection angle between beams of the same pair was approximately 2°.

After the coarse arrangement of the system, precise tuning was accomplished to achieve best sum-frequency beam overlap and highest conversion efficiency. Experimental investigation showed that after alignment, sum-frequency beams corresponding to fundamental beam pairs of channels 2+4 and 1+3 overlapped in space and composed single beam in which pulses are multiplexed in time (Fig. 26a). Measurement of conversions efficiency dependence on fundamental pulse energy showed that conversion efficiency well above 50 % could be achieved (Fig. 26b). Beam quality measurements of combined beam indicated that beam stays nearly diffraction limited up to the point of the highest conversion efficiency. Beyond this point, some deterioration in the beam irradiance distribution could be seen, as well as a reduction in conversion efficiency. This was relevant to both KTP and LBO nonlinear crystals.
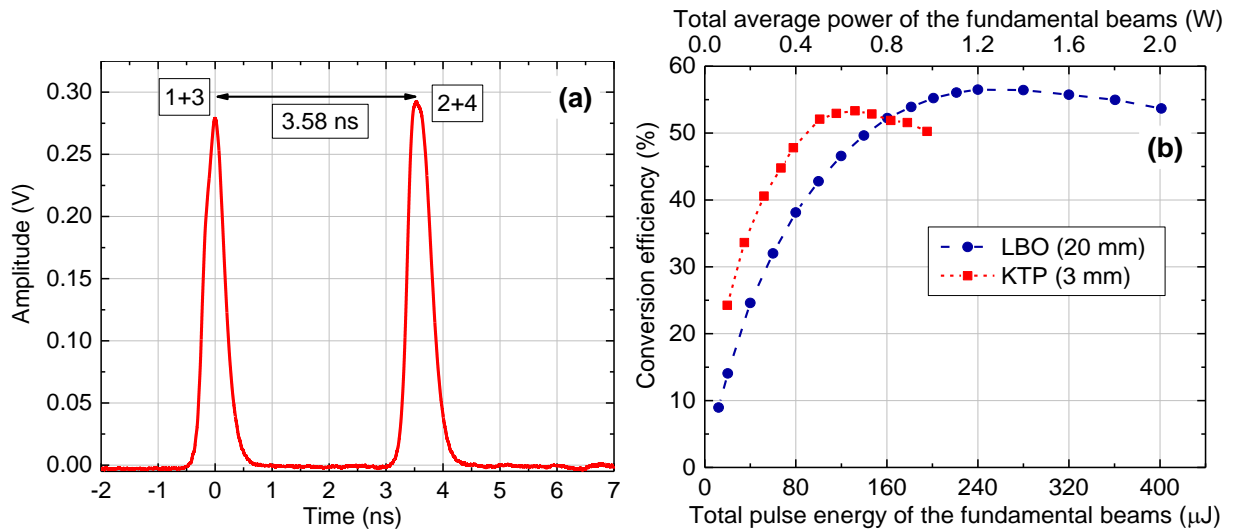
Fig. 26 (a) Time-domain pulse measurement of the combined beam (532 nm) achieved by using pulse source A and KTP crystal. Pulses generated from pairs 1+3 and 2+4 are marked in the figure. (b) Overall conversion efficiency versus total energy of the fundamental beams when combining amplified pulses from source A in KTP (red) and LBO (blue) crystal.

Highest average power in the combined beam was achieved using pulse source B and LBO nonlinear crystal. In this configuration, conversion efficiency up to 51 % and average power of 29 W in the combined beam was achieved (Fig. 27a). Beam quality of the combined beam, measured at the highest conversion efficiency operation point, was nearly diffraction limited (M^2_h=1.32 in the horizontal direction and M^2_v=1.16 in the vertical direction) (Fig. 27b).
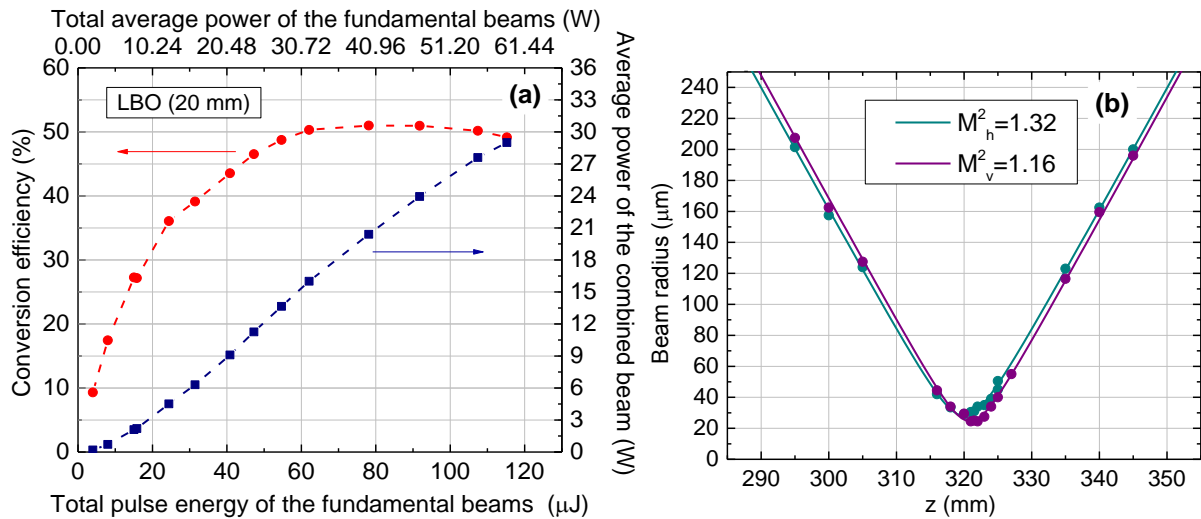
Fig. 27 (a) Overall conversion efficiency and average power in the combined beam versus total energy of the fundamental beams when combining amplified pulses from the source B in the LBO crystal. (b) $1/e^2$ beam radius measurement of the combined beam versus propagation distance (points). Measured at the optimal conversion efficiency operation point.

Sequential nonlinear pulse combining

Second pulse combining method is based on the property that sum-frequency generation takes place only when relevant pulses overlap in time, and phase-matching conditions are fulfilled. This allows arranging sum-frequency generation setup in such way that two fundamental pulses separated in time could be combined into the single sum-frequency pulse. The first pulse of the sequence passes through the crystal without nonlinear interaction, is directed back to the input of the crystal and during the second pass through the crystal, it overlaps with arriving the second pulse of the sequence (Fig. 28). Phase-matching conditions are fulfilled, and single sum-frequency pulse is generated. There are few possible implementations of this method. For type I phase-matching, the non-collinear configuration is required in which first and second passes through the crystal are arranged at different angles (Fig. 28a). For type II phase-matching, first and second passes of the pulses can be distinguished by the polarization. The first pulse of the sequence can be returned for the second pass back through the crystal (Fig. 28b) or by some different path (Fig. 28c). Former configuration was investigated experimentally.
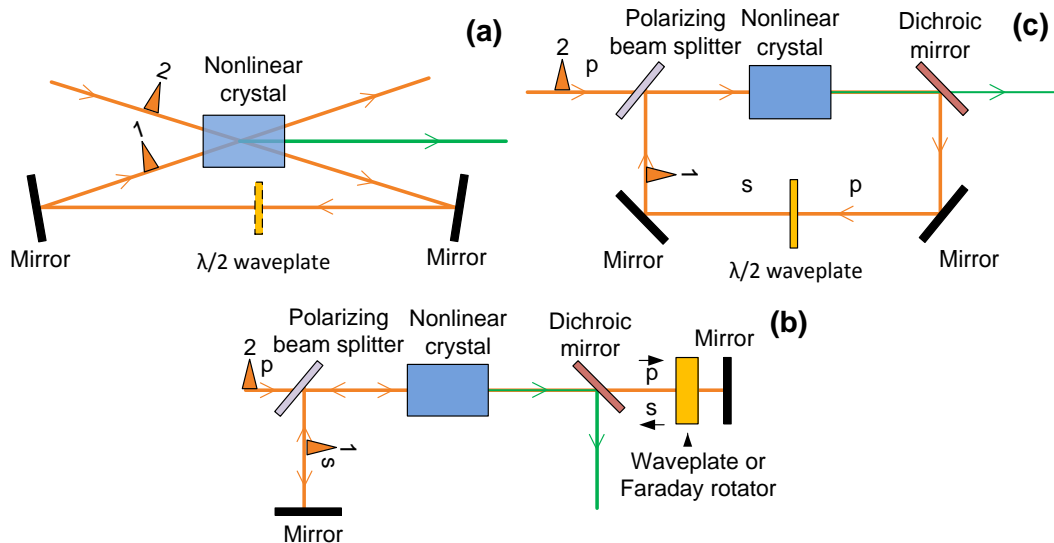
Fig. 28 Schematic diagrams of the sequential nonlinear pulse combining setups. Letters **s** and **p** indicate polarization states which are mutually orthogonal.

35

In the experimental setup, pulses from microchip laser (400 ps duration, 5 kHz repetition rate, 1064 nm wavelength) were used (Fig. 29). Sequences of two pulses were formed by using a polarizer, delay line and the beam splitter. The time delay between pulses was set according to requirements for latter pulse combining. Pulses were amplified in 30 µm core diameter LMA DC PM Yb-doped fiber, pumped in counter-propagating configuration. Amplified pulses were directed to the pulse combining scheme based on a nonlinear KTP crystal (length 4 mm, cut angle $\theta=90°$, $\varphi=24°$, interaction type II) (Fig. 29).
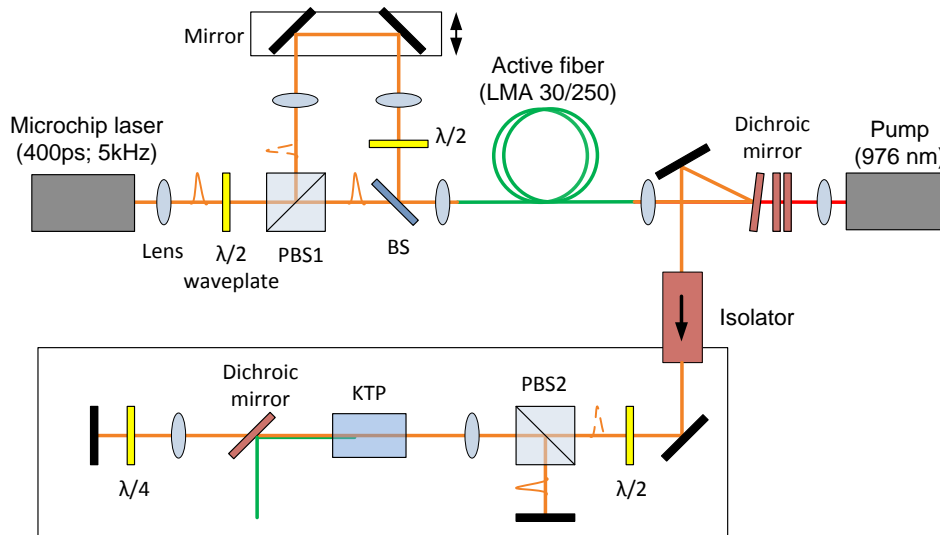
Fig. 29 Schematic diagram of the experimental setup. PBS – polarizing beam splitter, BS – beam splitter.

Pulses were amplified in the fiber amplifier up to ~100 µJ pulse energy before significant nonlinear effects appeared. After alignment of the pulse combining setup, two pulses in the sequence were successfully combined into single sum-frequency pulse (Fig. 30). No additional residual second harmonic pulses were observed (Fig. 30b).
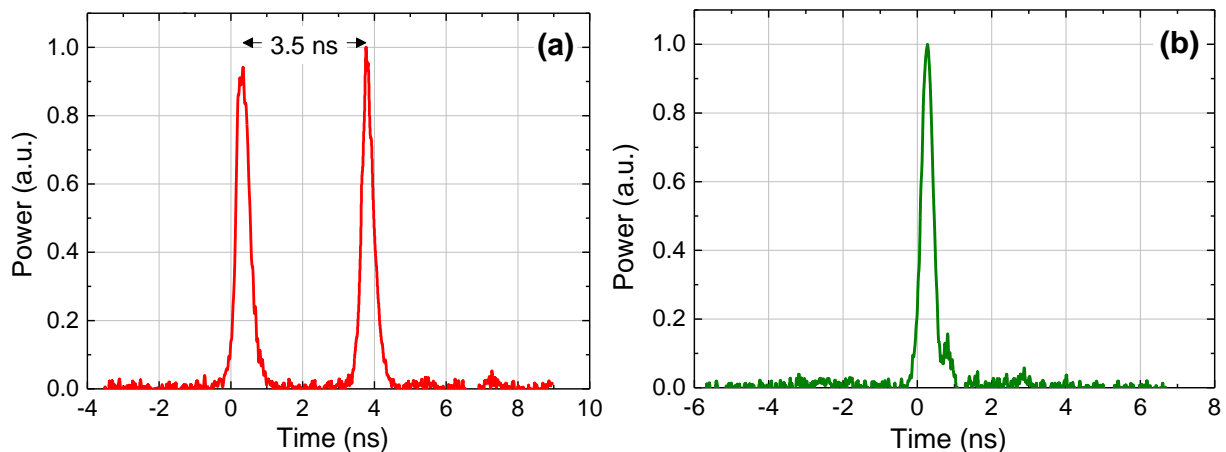
Fig. 30 Temporal envelopes of fundamental pulses (a) and sum-frequency pulse after combining (b).

The pulse energy of the combined sum-frequency pulses versus fundamental pulse energy is shown in Fig. 31. Results are compared with the conventional SHG. When pulses were combined, higher pulse energy (104 µJ) was achieved compared to the case when conventional SHG configuration was used (<80 µJ). Beam quality measurements of the combined beam showed no beam distortions ($M^2_{x/y} = 1,06/1,03$).

36
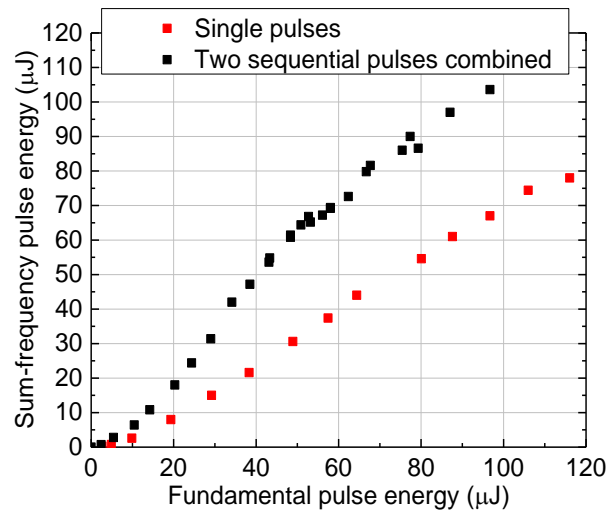
Fig. 31 Sum-frequency pulse energy dependence on pulse energy of the fundamental pulses. Black points – using pulse combining setup, red points – using conventional SHG setup.

Main results and conclusions

1. Stable ultrashort pulses with relatively high energy and wavelength in the range of Yb-doped fused silica can be generated by utilizing self-phase modulation in fiber and double-alternating spectral filtering.

Self-starting pulse generation can be achieved in such fiber laser circuits by setting correct spectral filter overlap or by implementing external resonator.

In pulse generator setup, in which influence of chromatic dispersion is low, pulse energy of stable pulse generation is inversely proportional to a full fiber length of the circuit and almost linearly proportional to the normalized spectral separation of the filter bands. The pulse duration of the generated pulses is inversely proportional to the filter bandwidth expressed in frequency units.

The operation of such pulse generator under conditions of normal chromatic dispersion is characterized by broader stability range with respect to gain. This property alleviates self-starting operation and allows to generate high-energy linearly-chirped pulses.

2. Nonlinear FCPA system in which self-phase modulation is utilized both in pulse stretcher and pulse amplification stages, after optimization, allows to generate pulses with a shorter duration than the duration of initial oscillator-seeder pulses, and with higher energy than achievable in linear operation regime for corresponding mode field area fiber.

The threshold of nonlinear effects in counter-propagating pumping configuration of the fiber amplifier can be tuned by changing signal power at the input of the fiber amplifier and gain in the fiber (pump power). In this configuration, the length of the active fiber has very small influence for the threshold of nonlinear effects. The opposite is observed in co-propagating pumping configuration, in which similar results can be achieved only after precise optimization of the fiber length.

In the LMA fiber, which can support multiple higher-order modes, the highest achievable pulse energy is limited by the four-wave mixing effect. In the nearly single-mode fiber, limitations caused by four-wave mixing are not observed, and achievable pulse energy per mode area is larger.

Polarization extinction ratio decreases with the increase of pulse energy in CCC technology fiber.

3. By using LBO crystal in the setup with a longitudinal temperature gradient, significantly higher conversion efficiency to the second harmonic of broadband pulses from fiber lasers can be achieved than using conventional SHG configuration in which crystal temperature is uniform.

In the setup with a longitudinal temperature gradient along LBO crystal, it is not necessary to optimize crystal length. The conversion process is unidirectional, back-conversion does not occur even when crystal length is much bigger than optimal.

By setting correct temperature gradient along LBO crystal, optical frequency conversion for radiation in the whole Yb-doped fused silica emission wavelength range (1000-1100 nm) can be accomplished.

4. Pulsed optical beams from multiple fiber amplifiers can be combined in pairs into a single beam in which pulses are multiplexed in time by using noncollinear sum-frequency

generation technique. The average power of the combined beam is proportional to the number of combined fiber amplifiers, and spatial characteristics of the combined beam are not worse than characteristics of beams generated in corresponding fiber amplifiers.

5.   Sequential pulse combining in quadratic susceptibility crystal allows generating sum-frequency pulses with higher energy and peak power than in the case when optical frequency conversion is accomplished using conventional SHG configuration.

Bibliography

1. S. B. Poole, D. N. Payne, and M. E. Fermann, "Fabrication of low-loss optical fibres containing rare-earth ions," Electronics Letters **21**, 737–738 (1985).
2. E. Snitzer, H. Po, F. Hakimi, R. Tumminelli, and B. C. McCollum, "Double clad, offset core Nd fiber laser," in *Optical Fiber Sensors (1988)* (Optical Society of America, 1988), p. PD5.
3. H. M. Pask, R. J. Carman, D. C. Hanna, A. C. Tropper, C. J. Mackechnie, P. R. Barber, and J. M. Dawes, "Ytterbium-doped silica fiber lasers: versatile sources for the 1-1.2 µm region," IEEE Journal of Selected Topics in Quantum Electronics **1**, 2–13 (1995).
4. J. D. Minelly, R. I. Laming, J. E. Townsend, W. L. Barnes, E. R. Taylor, K. P. Jedrzejewski, and D. N. Payne, "High-gain fiber power amplifier tandem-pumped by a 3-W multistripe diode," in *Digest of Conference on Optical Fiber Communication (1992)* (Optical Society of America, 1992), p. TuG2.
5. C. Jauregui, J. Limpert, and A. Tünnermann, "High-power fibre lasers," Nature Photonics **7**, 861–867 (2013).
6. J. D. Kafka, D. W. Hall, and T. Baer, "Mode-locked erbium-doped fiber laser with soliton pulse shaping," Optics Letters **14**, 1269–1271 (1989).
7. M. E. Fermann, M. Hofer, F. Haberl, and S. P. Craig-Ryan, "Femtosecond fibre laser," Electronics Letters **26**, 1737–1738 (1990).
8. C. D. Brooks and F. Di Teodoro, "Multimegawatt peak-power, single-transverse-mode operation of a 100µm core diameter, Yb-doped rodlike photonic crystal fiber amplifier," Applied Physics Letters **89**, 111119 (2006).
9. J. Limpert, F. Stutzki, F. Jansen, H.-J. Otto, T. Eidam, C. Jauregui, and A. Tünnermann, "Yb-doped large-pitch fibres: effective single-mode operation based on higher-order mode delocalisation," Light: Science & Applications **1**, e8 (2012).
10. L. Kuznetsova and F. W. Wise, "Scaling of femtosecond Yb-doped fiber amplifiers to tens of microjoule pulse energy via nonlinear chirped pulse amplification," Optics Letters **32**, 2671–2673 (2007).
11. T. Eidam, J. Rothhardt, F. Stutzki, F. Jansen, S. Hädrich, H. Carstens, C. Jauregui, J. Limpert, and A. Tünnermann, "Fiber chirped-pulse amplification system emitting 3.8 GW peak power," Optics Express **19**, 255–260 (2011).
12. T. Zhou, J. Ruppe, P. Stanfield, J. Nees, R. Wilcox, and A. Galvanauskas, "Resonant cavity based time-domain multiplexing techniques for coherently combined fiber laser systems," The European Physical Journal Special Topics **224**, 2585–2602 (2015).
13. M. Kienel, M. Müller, A. Klenke, J. Limpert, and A. Tünnermann, "12 mJ kW-class ultrafast fiber laser system using multidimensional coherent pulse addition," Optics Letters **41**, 3343 (2016).
14. L. Shah, M. E. Fermann, J. W. Dawson, and C. P. J. Barty, "Micromachining with a 50 W, 50 µJ, subpicosecond fiber laser system," Optics Express **14**, 12546–12551 (2006).
15. M. Mielke, "Ultrafast Fiber Laser Platform for Advanced Materials Processing," Journal of Laser Micro/Nanoengineering **5**, 53–58 (2010).
16. P. Gečys, G. Račiukaitis, E. Miltenis, A. Braun, and S. Ragnow, "Scribing of Thin-film Solar Cells with Picosecond Laser Pulses," Physics Procedia **12**, **Part B**, 141–148 (2011).

17. R. Mary, D. Choudhury, and A. K. Kar, "Applications of Fiber Lasers for the Development of Compact Photonic Devices," IEEE Journal of Selected Topics in Quantum Electronics **20**, 72–84 (2014).

18. C. Gu, M. Hu, L. Zhang, J. Fan, Y. Song, C. Wang, and D. T. Reid, "High average power, widely tunable femtosecond laser source from red to mid-infrared based on an Yb-fiber-laser-pumped optical parametric oscillator," Optics Letters **38**, 1820–1822 (2013).

19. S. Fan, H. Takeuchi, T. Ouchi, K. Takeya, and K. Kawase, "Broadband terahertz wave generation from a $MgO:LiNbO_3$ ridge waveguide pumped by a 1.5 μm femtosecond fiber laser," Optics Letters **38**, 1654–1656 (2013).

20. J. Adamonis, N. Rusteika, R. Danilevičius, and A. Krotkus, "A compact terahertz burst emission system driven with 1μm fiber laser," Optics Communications **293**, 61–64 (2013).

21. G. Mourou, B. Brocklesby, T. Tajima, and J. Limpert, "The future is fibre accelerators," Nature Photonics **7**, 258–261 (2013).

22. L. Tunna, A. Kearns, W. O'Neill, and C. J. Sutcliffe, "Micromachining of copper using Nd:YAG laser radiation at 1064, 532, and 355 nm wavelengths," Optics & Laser Technology **33**, 135–143 (2001).

23. G. Agrawal, *Nonlinear Fiber Optics, Third Edition* (Academic Press, 2001).

24. J. Lægsgaard, "Control of fibre laser mode-locking by narrow-band Bragg gratings," Journal of Physics B: Atomic, Molecular and Optical Physics **41**, 095401 (2008).

25. R. Paschotta, J. Nilsson, A. C. Tropper, and D. C. Hanna, "Ytterbium-doped fiber amplifiers," IEEE Journal of Quantum Electronics **33**, 1049–1056 (1997).

26. J. R. Marciante and J. D. Zuegel, "High-gain, polarization-preserving, Yb-doped fiber amplifier for low-duty-cycle pulse amplification," Applied Optics **45**, 6798–6804 (2006).

27. D. von der Linde, "Characterization of the noise in continuously operating mode-locked lasers," Applied Physics B **39**, 201–217 (1986).

28. E. Treacy, "Optical pulse compression with diffraction gratings," IEEE Journal of Quantum Electronics **5**, 454–458 (1969).

29. R. A. Haas, "Influence of a constant temperature gradient on the spectral-bandwidth of second-harmonic generation in nonlinear crystals," Optics Communications **113**, 523–529 (1995).

30. K. Kato, "Temperature-tuned 90° phase-matching properties of LiB_3O_5," IEEE Journal of Quantum Electronics **30**, 2950–2952 (1994).

31. A. V. Smith, R. J. Gehr, and M. S. Bowers, "Numerical models of broad-bandwidth nanosecond optical parametric oscillators," Journal of the Optical Society of America B **16**, 609–619 (1999).

32. G. Arisholm, "General numerical methods for simulating second-order nonlinear interactions in birefringent media," Journal of the Optical Society of America B **14**, 2543–2549 (1997).

33. C. Chen, Y. Wu, A. Jiang, B. Wu, G. You, R. Li, and S. Lin, "New nonlinear-optical crystal: LiB_3O_5," Journal of the Optical Society of America B **6**, 616–621 (1989).

34. Y. Furukawa, S. A. Markgraf, M. Sato, H. Yoshida, T. Sasaki, H. Fujita, T. Yamanaka, and S. Nakai, "Investigation of the bulk laser damage of lithium triborate, LiB_3O_5, single crystals," Applied Physics Letters **65**, 1480–1482 (1994).

Santrauka

Šioje disertacijoje buvo tiriami būdai impulsų generavimui ir stiprinimui iterbiu legiruotose kvarcinio stiklo skaidulose. Taip pat buvo tiriami metodai impulsinės spinduliuotės generuojamos skaidulinių lazerių optinio dažnio keitimui ir impulsinių pluoštų apjungimui pasinaudojant netiesine sąveika kvadratinio jautrio kristale. Visa tai reikalinga norint pritaikyti skaidulinių lazerių technologijas norimų laikinių, energetinių ir bangos ilgio parametrų impulsų generavimui.

Tiriamas impulsų generavimo metodas remiasi impulsų spektro plitimo dėl fazės moduliavimosi ir dvigubo-pakaitinio filtravimo panaudojimu. Atlikti skaitiniai modeliavimai ir eksperimentiniai tyrimai parodė, kad šis metodas leidžia generuoti stabilias ir santykinai didelės energijos optinių impulsų sekas. Šio impulsų generavimo metodo teikiami privalumai leidžia prognozuoti, kad ateityje tokiu pagrindu veikiantys lazeriai galėtų pakeisti įprastinius sinchronizuotų modų skaidulinius lazerius.

Impulsų stiprinimo skaiduloje tyrimai buvo atliekami taikant čirpuotų impulsų stiprinimo metodiką ir naudojant skirtingo šerdies diametro (ir technologijos) stiprintuvo skaidulas. Buvo pademonstruota nesudėtingos sandaros eksperimentinė netiesinė čirpuotų impulsų stiprinimo sistema, kurioje fazės moduliavimasis yra panaudojamas impulsų plėtimo pakopoje ir pagrindiniame skaiduliniame stiprintuve, kas leidžia generuoti itin trumpus ir didelės energijos impulsus (po suspaudimo).

Skaidulinių lazerių generuojamų plataus spektro impulsų optinio dažnio keitimui buvo pritaikytas antros harmonikos generavimo metodas, kai išilgai kvadratinio jautrio kristalo yra sudaromas temperatūros gradientas. Skaitiniai modeliavimai ir eksperimentiniai šio metodo tyrimai parodė, kad toks metodas leidžia padidinti plataus spektro impulsų optinio dažnio keitimo našumą lyginant su įprastine antros harmonikos generavimo konfigūracija.

Pasinaudojant suminio dažnio generavimo kvadratinio jautrio kristale nekolinearioje konfigūracijoje savybėmis, buvo pademonstruotas impulsinių pluoštų, sustiprintų keturiuose skaiduliniuose stiprintuvuose, apjungimas generuojant vieną suminio dažnio pluoštą, kuriame impulsai yra sutankinami laike. Eksperimentiniai šio metodo tyrimai parodė, kad impulsiniai pluoštai iš skaidulinių stiprintuvų gali būti apjungimai pasiekiant aukštą konvertavimo į suminį dažnį našumą ir išlaikant artimą difrakcijos ribotai pluošto kokybę. Apjungiant kelis pluoštus generuojamus skaidulinių lazerių gali būti padidinamas impulsų pasikartojimo dažnis ir vidutinė galia, kartu atliekant optinio dažnio keitimą.

Taikant dar kitą metodą, buvo apjungimai du laike atskirti impulsai, sustiprinti skaiduliniame stiprintuve, generuojant vieną suminio dažnio impulsą. Eksperimentinė šio metodo realizacija leido gauti didesnės energijos ir smailinės galios suminio dažnio impulsus negu taikant standartinę antros harmonikos generavimo konfigūraciją.

Curriculum Vitae

PERSONAL DETAILS

Name:	**Julijanas Želudevičius**
Date of birth:	1987.08.24
Place of birth:	Vilnius
E-mail:	j.zeludevicius@ar.fi.lt

EDUCATION

2012 – 2016	Center for physical sciences and technology, PhD studies, science field: material engineering (T08).
2010 – 2012	Vilnius University, Laser physics and optical technologies, Master of physics.
2006 – 2010	Vilnius University, Telecommunication physics and electronics, Bachelor of electronic engineering.
2002 – 2006	A.Mickevičiaus gymnasium, Vilnius.
1994 – 2002	Jono Pauliaus II secondary school, Vilnius.

WORK EXPERIENCE

2012 – now	Center for Physical Sciences and Technology, Department of Laser Technology – junior research fellow.
2011 – 2012	Center for Physical Sciences and Technology, Department of Laser Technology – engineer.
2008 – 2009	Center for Physical Sciences and Technology, Department of Laser Technology – technician.